

# Efficient method for the simulation of STM images. I. Generalized Green-function formalism

J. Cerdá\* and M. A. Van Hove†

*Materials Sciences Division, Lawrence Berkeley National Laboratory, University of California, Berkeley, California 94720*

P. Sautet

*Institut de Recherche sur la Catalyse, CNRS, 2 Avenue Albert Einstein, 69626 Villeurbanne, France  
and Laboratoire de Chimie Théorique, Ecole Normale Supérieure, 46 Allée d'Italie, 69364 Lyon Cedex 07, France*

M. Salmeron

*Materials Sciences Division, Lawrence Berkeley National Laboratory, University of California, Berkeley, California 94720*

(Received 3 June 1997)

We present a theoretical formalism specially suited for the simulation of scanning tunneling microscopy (STM) images. The method allows for a realistic description of the STM system, taking fully into account its three-dimensional nature. Bias effects may also be considered since the theory is not restricted to the low-bias limit. The starting point is the previously applied Landauer-Büttiker formula, which expresses the current at the STM junction as a sum of transmission coefficients linking eigenstates at each electrode. The transmission coefficients are directly obtained from the scattering matrix which is, in our approach evaluated through Green-function techniques; in particular, we employ the surface Green-function matching (SGFM) method to find the Green function at the interface, and explicitly derive simple expressions for the current. Additionally, the formalism goes beyond the elastic-scattering limit by considering inelastic effects via an optical potential. We also present a method to analyze the current in terms of contributions arising from individual atomic orbital interactions and their interference with other interactions. To this end, the SGFM method is replaced by a first-order expansion of the interface Green function. [S0163-1829(97)04648-1]

## I. INTRODUCTION

Since the early work of Tersoff and Hamann<sup>1</sup> on the theory of the scanning tunneling microscope (STM), many theoretical approaches have been developed in order to gain further physical insight into the real space images that this technique provides.<sup>2-6</sup> Most of the basic principles governing the current or topographic contrast recorded in a STM image are now reasonably well understood in terms of the electronic and atomic structures of both the tip and surface being probed together with their interactions.<sup>2</sup> Moreover, most STM-related experimental findings have also been satisfactorily explained, such as bias-dependent images,<sup>7</sup> negative differential resistances,<sup>8,9</sup> electron-density waves,<sup>10</sup> atom transport,<sup>11</sup> quantization of the conductance,<sup>12</sup> and thermovoltage measurements,<sup>13</sup> among many others.

There exist, however, few STM theories that can be used routinely to simulate STM images for a great variety of systems in a fast and simple way, and that are realistic enough to make a comparison with the experiment meaningful. It is often the case that a semiquantitative theory suffices to extract useful information from a STM image or from spectroscopic data, rather than performing accurate first-principles calculations which are usually time consuming or even intractable. Such an approach is necessary, for example, when one desires to monitor chemical reactions with the STM. It is then crucial to identify coadsorbed species before and after the reaction takes place. To determine the chemical identity or their adsorption sites is not often a trivial task that can be directly extracted from the experimental image, so that one needs to perform parallel calculations in order to assign dif-

ferent types of *bumps* or *holes* to a particular atom or molecule.

The so-called elastic-scattering quantum chemistry (ESQC) theory<sup>3,4,14-17</sup> has revealed itself as a computationally fast and convenient scheme to calculate theoretical STM images. Up to now, it has been successfully applied to a great variety of systems: CO adsorbed on Pt(111),<sup>14</sup> benzene on Pt(111) (Ref. 18) and on Rh(111),<sup>3</sup> O and several other atoms on Pt(111),<sup>15</sup> and S on Re(0001) (Ref. 16) and on Mo(100),<sup>17</sup> among others. In the ESQC approach, the conductance of the system is evaluated via the Landauer-Büttiker formula (LBF),<sup>19</sup> which connects electronic states (channels) on both sides of the STM junction. In this way, the coupling of the surface and the tip apex to their respective bulk materials is fully taken into account. The probability for electrons to be transmitted from one channel to another is directly obtained from the scattering matrix  $S$  which is, in turn, evaluated through the transfer-matrix technique<sup>3,20</sup> (TM). However, the TM can only be applied to symmetrical junctions in the sense that both the geometrical and electronic structures of the tip and substrate bulk materials have to be considered as identical. This requirement has also prevented the use of ESQC for analyzing spectroscopic data, since the applied bias shifts the energy bands at each side of the junction in opposite directions, thus breaking the symmetry. All previous studies using the ESQC theory have therefore been restricted to the low-bias limit which is, nevertheless, a common experimental condition when probing metallic samples.

In this paper we present a reformulation of the ESQC method, whereby in obtaining the scattering matrix  $S$  the TM

technique is replaced by the surface Green-function matching (SGFM) method.<sup>21</sup> A very similar approach, but restricted to the one-dimensional (1D) case and the low-bias limit, was recently developed by Chico *et al.*<sup>22</sup> in connection to the conductance of nanotube heterojunctions. As will be shown, the use of Green functions lifts all the above restrictions. At the same time, the full 3D nature of the system is also taken into account through an integration in  $\mathbf{k}$  space over the Brillouin zones of the substrate and tip. Furthermore, we show how a decomposition of the current into individual atomic-orbital contributions or interference terms may be accomplished if the SGFM method is replaced by a first-order perturbation theory. The actual application of the theory to some real systems, together with a detailed study of the effect of the parameters involved will be presented in the following paper.<sup>23</sup>

In Sec. II we will briefly explain how the LBF (Ref. 19) is applied to the STM problem. Although there exist more recent and general formalisms to the quantum transport,<sup>24</sup> we feel that the LBF formula offers a conceptually simple, yet correct approach to the problem. The complete theory for the one-dimensional case will be presented in Sec. III, where we also show its equivalence with the ESQC for a simple model. The extension to three dimensions and the method for the current analysis are described in Sec. IV, while in Sec. V we incorporate in an approximate way inelastic effects within the theory. We leave to Sec. VII a final discussion on the present STM formalism.

## II. LANDAUER FORMULA APPLIED TO THE STM

As depicted in Fig. 1(a), we model the STM experimental setup by two perfect conducting wires corresponding to the substrate  $s$  and the tip  $t$ . Each wire has one of its terminations attached to an electron reservoir characterized by chemical potentials  $\mu_s$  and  $\mu_t$ , respectively. The two wires are then brought close to each other forming an interface  $\mathcal{I}$  which we identify as the STM junction. Since the electronic and geometrical structures of the sample and tip surfaces will in general differ from those within their corresponding bulk materials, it is convenient to define each surface as a separate block which we denote by  $r$  for the *reconstructed* termination of the  $s$  wire, and by  $a$  for the tip apex of the  $t$  wire. The interface  $\mathcal{I}$  is thus composed of the two surface blocks  $r$  and  $a$ .

In the STM experiment, the difference in chemical potentials at the  $s$  and  $t$  reservoirs is externally controlled through the applied sample bias  $V$ , so that  $eV = \mu_s - \mu_t$  (with  $e < 0$ ), and an electron flow sets up from the wire at higher chemical potential to the wire at lower potential. This situation is illustrated in Fig. 1(b) for the case  $\mu_t > \mu_s$ , which corresponds to a positive sample bias  $V$  ( $eV < 0$ ). In order to evaluate the current  $I(V)$  associated with this flow we follow the arguments of Büttiker *et al.*,<sup>19</sup> considering the zero-temperature limit. At a given energy  $E$ , each wire  $\alpha$ , where  $\alpha = s$  and  $t$ , may be described by a certain number  $N_\alpha(E)$  of independent ideal one-dimensional conductors, which are referred to as channels. Electrons propagate through these channels without dissipation from the reservoirs to their respective surfaces, and vice versa. We may denote each channel  $m$  by the ket  $|u_\alpha^{\pm m}(E)\rangle$ , where we use the  $+$  sign for propagation from

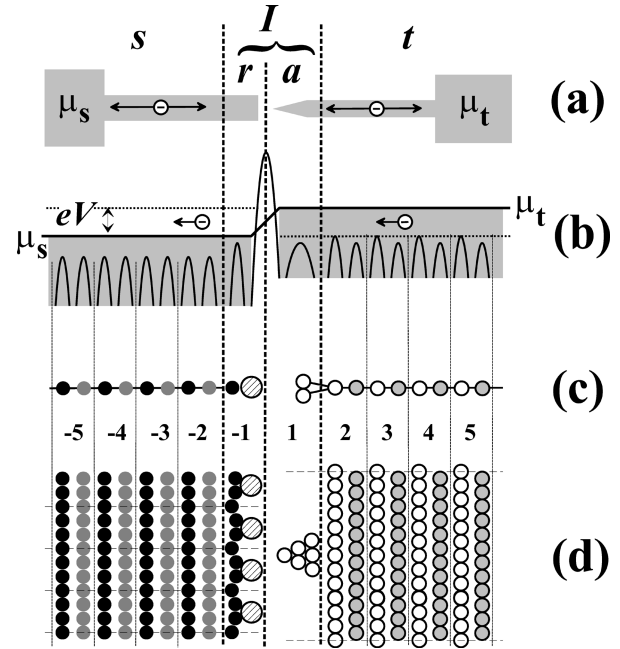


FIG. 1. Schematic of the STM theoretical model. (a) The substrate  $s$  and tip  $t$  are considered as wires connected to a reservoir. (b) Chemical potential  $\mu$  at each wire when a negative bias  $V$  is set between the two reservoirs. All allowed states below  $\mu$  are assumed to be occupied. The atomic-scale potential energy along the wires and at the junction is also sketched as curved lines. (c) The 1D model: the numbering below each pair of atoms denotes the principal layers (PL's). (d) The 3D model: dashed horizontal lines indicate the surface superlattices at  $r$  and  $a$ , which are taken commensurate with their respective bulk lattices.

$s$  to  $t$  and the  $-$  sign for the opposite direction. The superscript  $m$ , which takes values between 1 and  $N_\alpha(E)$ , stands for any proper quantum number such as the band index (this will be clarified in the next sections). Notice that the flow directions at both bulk materials need not be along the same axis, but it will be determined by the particular shape and relative orientation of the wires. In particular, the bulk repeat vectors at the two wires might not be aligned with each other, although in Fig. 1(a) they are depicted in such an arrangement. At  $T=0$ , the reservoirs will inject electrons into the channels so that they are all occupied up to their respective chemical potentials and unoccupied for higher energies. All the chemical potential drop is assumed to be localized in the vacuum region of the junction [Fig. 1(b)]. We can then view an electron in channel  $|u_t^{-m}(E)\rangle$  propagating along the  $t$  bulk material until it reaches the interface  $\mathcal{I}$  where it is scattered, having certain probability  $\langle u_s^{-m'}(E') | \mathcal{T} | u_t^{-m}(E) \rangle$  to transmit across the junction into channel  $|u_s^{-m'}(E')\rangle$  at  $s$  or  $\langle u_t^{+m'}(E') | \mathcal{R} | u_t^{-m}(E) \rangle$  for back reflecting into another channel at  $t$ . Depending on the energy  $E'$  of the scattered electron the scattering process may either be elastic ( $E=E'$ ) or inelastic ( $E \neq E'$ ). Next, we take the elastic-scattering limit and approximate the transmission probabilities by

$$\begin{aligned} \langle u_s^{-m'}(E') | \mathcal{T} | u_t^{-m}(E) \rangle &\approx \delta(E-E') \langle u_s^{-m'}(E') | \mathcal{T} | u_t^{-m}(E) \rangle \\ &= \delta(E-E') \mathcal{T}_{m',m}^-(E). \end{aligned} \quad (1)$$

The first equality in Eq. (1) implies that all the scattering at  $\mathcal{I}$  is elastic, the contribution to the transmission arising from dissipative processes being neglected. The great advantage in using this approach is that only the energy range  $[\mu_s, \mu_s - eV]$  needs to be considered when evaluating the current; channels at  $t$  with energies below  $\mu_s$  cannot transmit into any channel at  $s$ , since they are all occupied at these energies. On the other hand, there will be no occupied channels at  $t$  above  $\mu_t = \mu_s - eV$ . A more detailed discussion of this limit will be given later in Sec. V. Under all the above assumptions, we may now use the many-channel LBF (Ref. 19) to evaluate the intensity across the junction:

$$I(V) = \frac{e}{\pi\hbar} \int_0^{-eV} dE \sum_{mm'} \mathcal{T}_{m',m}^-(E + \mu_s), \quad V > 0. \quad (2)$$

If the sample bias is reversed ( $\mu_s > \mu_t$ ), then the electron flow will be directed from  $s$  to  $t$ , and the same reasoning will lead to a similar expression for the current flowing in the opposite direction:

$$I(V) = \frac{e}{\pi\hbar} \int_0^{-eV} dE \sum_{mm'} \mathcal{T}_{m',m}^+(E + \mu_s), \quad V < 0, \quad (3)$$

where  $eV$  now takes positive values.

In deriving Eqs. (2) and (3) it is further assumed that channels are normalized to unit flux, so that the current fed into any channel is independent of its group velocity.

The key ingredient in evaluating  $I(V)$  is therefore the transmission probability matrix  $\mathcal{T}^\pm(E)$  which couples channels on each side of the interface. These probabilities are related to the scattering matrix  $\mathcal{S}^\pm(E)$  through the following relation:<sup>25,26</sup>

$$\mathcal{T}_{m',m}^\pm(E) = |\langle u_{\alpha'}^{\pm m'}(E) | \mathcal{S}^\pm(E) | u_\alpha^{\pm m}(E) \rangle|^2 \frac{v_{\alpha'}^{m'}}{v_\alpha^m}. \quad (4)$$

here  $\alpha$  and  $\alpha'$  stand for  $s$  or  $t$  depending on the transmission direction, and  $v_\alpha^m$  is the group velocity of channel  $m$ . The last factor in Eq. (4) accounts for the flux normalization at each channel.

The whole problem is thus reduced to the evaluation of the scattering matrix  $\bar{\mathcal{S}}^\pm(E)$  in the *channel basis*, whose elements we define as

$$\bar{\mathcal{S}}_{m',m}^\pm(E) = \langle u_{\alpha'}^{\pm m'}(E) | \mathcal{S}^\pm(E) | u_\alpha^{\pm m}(E) \rangle. \quad (5)$$

The next two sections are devoted to obtaining explicit expressions for these matrix elements.

### III. 1D CASE

#### A. Definitions and notations

For the one-dimensional case we regard each wire as a semi-infinite chain where the side extending to infinity corresponds to the one attached to the reservoir. A scheme of the model is illustrated in Fig. 1(c). Although we denote this system as 1D, it is in fact more general than just a simple linear chain, since we allow the wires to have a finite lateral

size (see, for example, block  $a$  in the figure). In analogy with Lee and Joannopoulos,<sup>20</sup> we split each chain into a semi-infinite stack of principal layers, where a principal layer (PL) is defined as the smallest group of atoms such that only nearest-neighbor interactions between PL's exist. We further assume that the bulk chains  $s$  and  $t$  can be described by a periodic array of identical PL's within each chain. As shown in Fig. 1(c), the numbering of PL's runs in increasing order from the  $s$  chain to the  $t$  chain, and the origin is chosen so that the two surface blocks  $r$  and  $a$  are located at PL's  $n = -1$  and  $1$ , respectively, while the PL  $n = 0$  is skipped. We therefore have  $n < -1$  for the  $s$  chain and  $n > 1$  for the  $t$  chain.

Within a linear combination of atomic orbitals framework, any wave function at any PL may be expanded in terms of a given set of atomic orbitals  $\{\alpha_i, i = 1, N_\alpha\}$ , and we allow different basis sets at each block. That is, at the surfaces we have the basis set  $\{r_i, i = 1, N_r\}$  at  $r$  and the set  $\{a_i, i = 1, N_a\}$  at  $a$ . In the bulk chains we have the set  $\{t_i, i = 1, N_t\}$  for  $n > 1$  and the set  $\{s_i, i = 1, N_s\}$  for  $n < -1$ . We emphasize that, as opposed to the TM technique where the  $\{s_i\}$  and  $\{t_i\}$  basis must be identical, in the present formalism the sizes of the four basis sets can be different, and this allows for a more realistic description of the system.

For a given energy  $E$ , wave functions at each PL  $n$  may be written as

$$|a_n(E)\rangle = \sum_{i=1}^{N_\alpha} a_{i,n}(E) |\alpha_i(\vec{d}_n)\rangle, \quad (6)$$

where now  $\alpha = t, a, r, s$  depending on the block in which PL  $n$  is located. The ket  $|\alpha_i(\vec{d}_n)\rangle$  corresponds to the  $i$ th orbital of the  $\{\alpha_i\}$  basis set located in PL  $n$ . The vector  $\vec{d}_n$  gives the origin of the PL.

We use a tight-binding Hamiltonian  $H$  with only nearest-neighbor interactions among PL's to describe the electronic part of the whole system. The infinite tridiagonal matrix  $H$  is sketched in Fig. 2(a). It consists of matrix blocks  $H_{nn'}$ , with  $n' = n, n \pm 1$  that give the interaction between PL's  $n$  and  $n'$ . A general matrix element at each  $nn'$  matrix block  $H_{nn'}(\alpha_i, \alpha'_j) = \langle \alpha_i(\vec{d}_n) | H | \alpha'_j(\vec{d}_{n'}) \rangle$  contains the interaction between orbital  $\alpha_i$  at  $n$  and  $\alpha'_j$  at  $n'$ . Obviously, if  $n$  and  $n'$  belong to the same bulk block  $s$  or  $t$ , these matrices will be independent of  $n$ , and we can replace the subscript  $n$  by  $s$  or  $t$  [see Fig. 2(a)].

In order to apply the LBF, Eqs. (2) and (3), we must first identify the channels  $|u_\alpha^{\pm m}(E)\rangle$ . Since the bulk chains  $s$  and  $t$  are assumed periodic, their eigenfunctions correspond to Bloch waves  $|\theta_\alpha^{\pm m}(E)\rangle$  characterized at each energy  $E$  by the quantities  $\theta_\alpha^{\pm m}(E) = k_\alpha^{\pm m}(E) a_\alpha$ , where  $a_\alpha$  is the lattice constant for the PL's and  $k_\alpha^{\pm m}(E)$  is the wave number giving the energy dispersion of the  $m$  energy band in chain  $\alpha$ . From now on we regard  $a_\alpha$  as a unit distance, and identify  $\theta_\alpha^{\pm m}(E)$  with the wave number along the propagation direction. These Bloch waves act precisely as the propagative channels for the electrons in the wires, each one with a group velocity given by

$$v_\alpha^m(E) = \frac{1}{\hbar} \frac{\partial E}{\partial \theta_\alpha^m}, \quad (7)$$

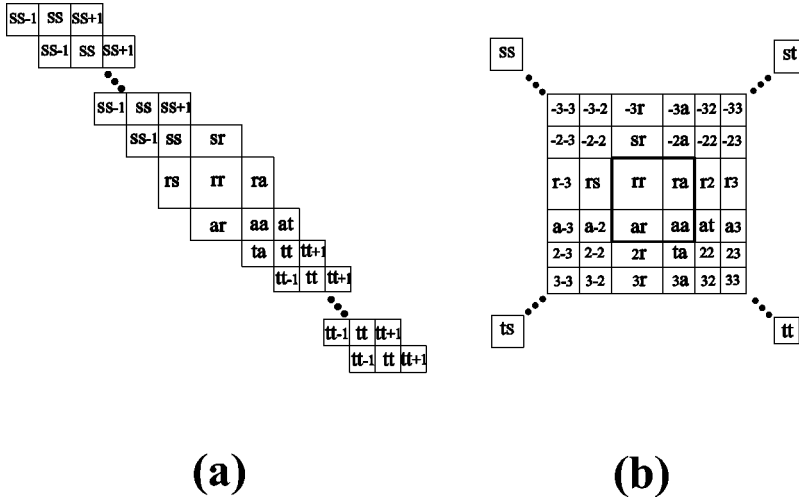


FIG. 2. Schematics and notation for the matrix blocks corresponding to (a) the Hamiltonian  $H$  and overlap matrix  $O$  and (b) the Green function  $\mathcal{G}$  for the 1D system of Fig. 1(c). The interface Green function  $\mathcal{G}_{II}$  is indicated by the central square in (b).

where the sign of the energy derivative determines the  $\pm$  direction of propagation in the channel.

The wave function of an electron in channel  $\pm m$  may then be written as

$$|\theta_{\alpha}^{\pm m}(E)\rangle = \frac{1}{\sqrt{N_{n,|n|>2}}} \sum_{|n|>2} |u_n^{\pm m}(E)\rangle, \quad (8)$$

$N$  being the number of PL's in the bulk material  $\alpha$ , while the kets  $|u_n^{\pm m}(E)\rangle$  give the wave-function amplitude of an electron at PL  $n$ , with  $|n|>2$ :

$$|u_n^{\pm m}(E)\rangle = \sum_{i=1}^{N_{\alpha}} u_{i,n}^{\pm m}(E) |\alpha_i(\vec{d}_n)\rangle, \quad (9)$$

which, since it must satisfy the Bloch condition, is related to adjacent PL's through

$$|u_{n\pm 1}^{+m}(E)\rangle = e^{\pm i\theta_{\alpha}^{+m}(E)} |u_n^{+m}(E)\rangle, \quad (10)$$

$$|u_{n\pm 1}^{-m}(E)\rangle = e^{\mp i\theta_{\alpha}^{-m}(E)} |u_n^{-m}(E)\rangle. \quad (11)$$

The interchannel scattering matrix elements  $\bar{S}_{m'm}^{\pm}(E)$  defined in Eq. (5) may then be obtained by relating Bloch wave amplitudes at PL's  $n$  and  $n'$  such that they are both at different bulk chains and far away from the interface:

$$\bar{S}_{m'm}^{+}(E) = \langle u_{n'}^{+m'}(E) | \mathcal{S} | u_n^{+m}(E) \rangle, \quad n' \gg 2, \quad n \ll -2, \quad (12)$$

$$\bar{S}_{m'm}^{-}(E) = \langle u_{n'}^{-m'}(E) | \mathcal{S} | u_n^{-m}(E) \rangle, \quad n' \ll -2, \quad n \gg 2, \quad (13)$$

where the requirement for both  $n$  and  $n'$  to be located deep inside the bulk materials ensures that any evanescent waves will make a negligible contribution to the scattering matrix.<sup>19</sup>

We now define the system's Green function  $\mathcal{G}(E)$  at a given complex energy  $E$  by

$$\mathcal{G}(E)F(E) = F(E)\mathcal{G}(E) = I, \quad (14)$$

where  $I$  is the identity matrix, and  $F(E)$  is the usual secular matrix defined as

$$F(E) = EO - H, \quad (15)$$

$H$  being the Hamiltonian and  $O$  the overlap matrix whose structure is identical to  $H$  [Fig. 2(a)]. To avoid divergences, the energy  $E$  is taken complex and a small positive imaginary part  $\delta$  is added to the actual real energy  $E_r$ :

$$E = E_r + i\delta. \quad (16)$$

It should be noted, however, that the formalism developed below is still numerically stable for values of  $\delta$  as low as  $10^{-10}$  eV, so that the use of a complex energy does not imply a limitation to the elastic-scattering approximation. The use of larger values for  $\delta$  will be discussed in Sec. V.

Any element of  $F$  may be written as

$$F_{nn'}(\alpha_i, \alpha'_j) = EO_{nn'}(\alpha_i, \alpha'_j) - H_{nn'}(\alpha_i, \alpha'_j), \quad (17)$$

where we have omitted the energy dependence of  $F$  for the sake of clarity, and we will maintain this convention for most of the matrix expressions appearing in the remaining sections. However, it is important to notice that under an applied bias  $V$  the energy levels at the chains shift in energy, so that the actual value of  $E$  to be used in Eq. (17) will be different whether we consider the  $rs$  or  $at$  sides of the junction. For the former, we use  $E_{rs} = E_F(s) + eV + E$ , while for the latter we have  $E_{at} = E_F(t) + eV + E$ , where  $E_F(\alpha)$  is the Fermi level of the  $\alpha$  bulk chain. As indicated in Sec. II,  $E$  ranges between 0 and  $-eV$ . This scheme ensures that both Fermi levels will be aligned for the zero bias case. As for the interblock  $F_{ar}$  and  $F_{ra}$  matrices we approximate the energy to a fixed value  $E_{ar} = \frac{1}{2}[E_F(s) + E_F(t)]$  independent of  $E$ . We believe that more sophisticated approaches to the evaluation of  $E_{ar}$ , which would take into account the specific shape of the potential drop at the junction, will not modify the final contrast in the image significantly. Besides, corrections to  $E_{ar}$  should be relatively small since this term multiplies the overlap matrices  $O_{ar}$  and  $O_{ra}$ , whose elements already have small values.

The structure of  $\mathcal{G}$  is shown in Fig. 2(b). The projection of Eq. (14) on any matrix block  $nn'$  yields two matrix equations depending on whether we use the first or second equal-

$$I\delta_{nn'} = F_{nn-1}\mathcal{G}_{n-1n'} + F_{nn}\mathcal{G}_{nn'} + F_{nn+1}\mathcal{G}_{n+1n'}, \quad (18)$$

$$I\delta_{nn'} = \mathcal{G}_{nn'-1}F_{n'-1n'} + \mathcal{G}_{nn'}F_{n'n'} + \mathcal{G}_{nn'+1}F_{n'+1n'}. \quad (19)$$

In order to evaluate  $\mathcal{G}$ , we use the Dyson equation, and choose as the unperturbed system that formed by the two semi-infinite chains (*ta* and *rs*) but assuming there is no interaction among them. Therefore, the unperturbed Hamiltonian and overlap matrices  $H^0$  and  $O^0$  will be identical to  $H$  and  $O$  except that the blocks *ra* and *ar* are set to zero. Since the chains are decoupled, the unperturbed Green function  $\mathcal{G}^0$  may be calculated separately for each one, and the problem reduces to evaluate the surface Green functions  $\mathcal{G}_{aa}^0$  and  $\mathcal{G}_{rr}^0$  and their couplings to their respective bulk chains. Notice that any matrix block  $\mathcal{G}_{nn'}^0$ , linking PL's  $n$  and  $n'$  that are not located in the same chain will be zero. The evaluation of  $\mathcal{G}^0$  is presented in Appendix A, and here we assume it to be known. The perturbation is then introduced by switching on the *ra* interactions that couple both chains. Since this perturbation is localized at the interface  $\mathcal{I}=r$  and  $a$ , to obtain  $\mathcal{G}$  from  $\mathcal{G}^0$ , we follow Ref. 21 and apply the SGFM method, generalizing it to nonorthogonal basis sets. By projecting the Dyson equation at  $\mathcal{I}$ , an expression for the interface Green function  $\mathcal{G}_{\mathcal{I}\mathcal{I}}$  can be easily deduced:

$$\mathcal{G}_{\mathcal{I}\mathcal{I}} = \begin{pmatrix} \mathcal{G}_{rr} & \mathcal{G}_{ra} \\ \mathcal{G}_{ar} & \mathcal{G}_{aa} \end{pmatrix} = \begin{pmatrix} (\mathcal{G}_{rr}^0)^{-1} & F_{ra} \\ F_{ar} & (\mathcal{G}_{aa}^0)^{-1} \end{pmatrix}^{-1}. \quad (20)$$

Knowledge of  $\mathcal{G}_{\mathcal{I}\mathcal{I}}$  and  $\mathcal{G}_0$  enables the evaluation of any  $\mathcal{G}_{n'n}$  matrix block through<sup>21</sup>

$$\mathcal{G}_{n'n} = \mathcal{G}_{n'n}^0 + \mathcal{G}_{n'i'}^0 (\mathcal{G}_{i'i'}^0)^{-1} (\mathcal{G}_{i'i}^0 - \mathcal{G}_{i'i}^0) (\mathcal{G}_{ii}^0)^{-1} \mathcal{G}_{in}^0, \quad (21)$$

where  $i$  and  $i'$  stand for the surface blocks *r* or *a* of the chains to which  $n$  and  $n'$  belong.

Any wave function  $|a_{n'}\rangle$  at any PL  $n'$  may now be obtained from the unperturbed wave function  $|a_n^0\rangle$  at  $n$  via the Lippman-Schwinger equation

$$|a_{n'}\rangle = \mathcal{G}_{n'n} (\mathcal{G}_{nn}^0)^{-1} |a_n^0\rangle. \quad (22)$$

Expressions (21) and (22) may be simplified by introducing the  $T_{nn'}$  and  $S_{nn'}$  transfer matrices

$$T_{n'n} = \mathcal{G}_{n'n}^0 (\mathcal{G}_{nn}^0)^{-1}, \quad (23)$$

$$S_{nn'} = (\mathcal{G}_{nn}^0)^{-1} \mathcal{G}_{nn'}^0, \quad (24)$$

so that we arrive at

$$|a_{n'}\rangle = T_{n'n} |a_n^0\rangle + T_{n'i'} (\mathcal{G}_{i'i}^0 - \mathcal{G}_{i'i}^0) S_{in} (\mathcal{G}_{nn}^0)^{-1} |a_n^0\rangle. \quad (25)$$

The interpretation of Eq. (25) is straightforward. The first term propagates  $|a_n^0\rangle$  from  $n$  to  $n'$ . Since  $T_{n'n}$  only depends on  $\mathcal{G}^0$  [see Eq. (23)], it can be readily identified with the unperturbed wave function  $|a_{n'}^0\rangle$  at that layer. It is worth noting that  $T_{n'n}$  should not be confused with the bulk transfer matrix  $(T_{s\pm 1s})^n$  appearing in Eq. (A10). According to our choice of the unperturbed system, we are also considering in  $T_{n'n}$  the scattering arising from the surface  $i$  (which is in the same chain as  $n$ ), although the presence of the other chain is

not taken into account. Obviously, if  $n$  and  $n'$  are located at different sides of the interface,  $|a_{n'}^0\rangle$  is zero. The second term in Eq. (25) adds to the first one the perturbation introduced by the other chain by first propagating  $|a_n^0\rangle$  to  $i$ , where it scatters to  $i'$  and finally it is propagated to  $n'$ . If  $i=i'$  (that is,  $n$  and  $n'$  are in the same chain) then Eq. (25) gives the reflected amplitude, while if  $i \neq i'$  ( $n$  and  $n'$  are at different chains) we obtain the transmitted amplitude. The scattering matrix  $\mathcal{S}$  relating the unperturbed wave function at  $n$  with the scattered wave at  $n'$  can then be directly extracted from this second term,

$$S_{n'n} = T_{n'i'} (\mathcal{G}_{i'i}^0 - \mathcal{G}_{i'i}^0) S_{in} (\mathcal{G}_{nn}^0)^{-1}. \quad (26)$$

## B. Scattering matrix in the Bloch basis

Since we are interested in the transmitted amplitudes, we need to consider in Eq. (26) the case where  $n$  and  $n'$  are located at different sides of the interface  $\mathcal{I}$  and, again, we will focus on the transmission along the negative direction, which corresponds to electrons propagating from the tip  $t$  to the substrate  $s$ . We then have  $i=a$ , and  $i'=r$ , and, taking the limits  $n \gg 2$  and  $n' \ll -2$ , Eq. (26) reads

$$S_{n'n}^- = T_{n'r} \mathcal{G}_{ra} S_{an} (\mathcal{G}_{tt}^0)^{-1}, \quad (27)$$

where we took into account that  $\mathcal{G}_{ra}^0 = 0$  for the unperturbed system, and  $\mathcal{G}_{nn}^0$  has been replaced by the  $t$  bulk diagonal Green-function matrix block  $\mathcal{G}_{tt}^0$ , since we are considering the limit  $n \gg 2$ .

Let us first decompose the transfer matrices  $T_{n'r}$  and  $S_{an}$  in the following forms:

$$\begin{aligned} T_{n'r} &= T_{n'n'+1} T_{n'+1n'+2} \cdots T_{-3-2} T_{-2r} \\ &= (T_{s-1s})^{-n'-2} T_{sr}, \end{aligned} \quad (28)$$

$$S_{an} = S_{a2} S_{23} \cdots S_{n-2n-1} S_{n-1n} = S_{at} (S_{tt+1})^{n-2}, \quad (29)$$

where we used the bulk transfer matrices  $T_{s-1s}$  and  $S_{tt+1}$  derived in Appendix A. The two second equalities in Eqs. (28) and (29) reflect the fact that transfer matrices  $T_{nn'}$  ( $S_{nn'}$ ) only depend on  $n-n'$  if both  $n$  and  $n'$  are in the same bulk block  $s$  or  $t$ , and  $n'$  is closer to (further from) the surface than  $n$  (see Appendix A). Using the latter expansions, Eq. (27) can be written as

$$S_{n'n}^- = (T_{s-1s})^{-n'-2} T_{sr} \mathcal{G}_{ra} S_{at} (S_{tt+1})^{n-2} (\mathcal{G}_{tt}^0)^{-1}, \quad (30)$$

or, using relation (A12), we may express the  $S_{tt+1}$  bulk transfer matrix in terms of  $T_{t-1t}$ :

$$S_{n'n}^- = (T_{s-1s})^{-n'-2} T_{sr} \mathcal{G}_{ra} S_{at} (\mathcal{G}_{tt}^0)^{-1} (T_{t-1t})^{n-2}. \quad (31)$$

For transmission along the positive direction we take the limits  $n \ll -2$  and  $n' \gg 2$  to arrive at a very similar relation,

$$S_{n'n}^+ = (T_{t+1t})^{n'-2} T_{ta} \mathcal{G}_{ar} S_{rs} (\mathcal{G}_{ss}^0)^{-1} (T_{s+1s})^{-n-2}. \quad (32)$$

These are our final relations for the scattering matrix  $S_{n'n}^\pm$  in the atomic-orbital (AO) basis.  $\mathcal{G}_{ra}$  or  $\mathcal{G}_{ar}$  are obtained from Eq. (20), and explicit expressions for the rest of the matrices appearing in Eqs. (31) and (32) are provided in

Appendix A. However, we still need to find the Bloch basis in order to transform  $\mathcal{S}_{n'n}^{\pm}$ . To this end, it is convenient to cast the Bloch coefficients appearing in Eq. (9) into vector form according to

$$\vec{u}_n^{\pm m} = (u_{1,n}^{\pm m}, u_{2,n}^{\pm m}, \dots, u_{N_\alpha,n}^{\pm m}). \quad (33)$$

By applying Eq. (A10) at any site  $n$  of the bulk chains, we have

$$\vec{u}_{n\pm 1}^{\pm m} = T_{\alpha\pm 1\alpha} \vec{u}_n^{\pm m}, \quad (34)$$

with  $\alpha = t, s$ . Comparing Eqs. (34) with Eqs. (10) and (11), we arrive at the following eigenvalue problem:

$$T_{\alpha\pm 1\alpha} \vec{u}_n^{\pm m} = e^{i\theta_\alpha^{\pm m}} \vec{u}_n^{\pm m}, \quad (35)$$

which implies that the reduction of the  $T_{\alpha\pm 1\alpha}$  into a diagonal form directly provides the wave numbers  $\theta_\alpha^{\pm m}$ :

$$T_{\alpha\pm 1\alpha} U_\alpha^\pm = U_\alpha^\pm \Theta_\alpha^\pm. \quad (36)$$

Here  $\Theta_\alpha^\pm$  is the diagonal matrix whose nonzero elements are the  $e^{i\theta_\alpha^{\pm m}}$  quantities, and the transformation matrix  $U_\alpha^\pm$  contains the Bloch eigenvectors

$$U_\alpha^\pm = (\vec{u}_n^{\pm 1}, \vec{u}_n^{\pm 2}, \dots, \vec{u}_n^{\pm N_\alpha}). \quad (37)$$

If  $\theta_\alpha^{\pm m}$  is real, we then have a propagative channel, while if it has a nonzero imaginary part the eigenstate corresponds to an evanescent wave which decays exponentially as we propagate from  $n$  to  $n \pm 1$ . We may now substitute Eq. (36) into Eq. (31) to obtain a more convenient expression for the scattering matrix  $\mathcal{S}_{n'n}^-$ :

$$\begin{aligned} \mathcal{S}_{n'n}^- &= U_s^- \{ (\Theta_s^-)^{-n'-2} (U_s^-)^{-1} T_{sr} \mathcal{G}_{ra} S_{at} (\mathcal{G}_{tt}^0)^{-1} \\ &\quad \times U_t^- (\Theta_t^-)^{n-2} \} (U_t^-)^{-1}. \end{aligned} \quad (38)$$

The braced factor in Eq. (38) can be easily identified with the scattering matrix in the Bloch basis  $\bar{\mathcal{S}}^-$ , which we were seeking. When considering limits (12) and (13) for  $n$  and  $n'$  in these expressions, the evanescent waves make a negligible contribution, and we may retain only those  $\bar{\mathcal{S}}_{m'm}^\pm$  matrix elements that relate the propagative channels  $m$  and  $m'$ . Furthermore, when taking the square modulus of these expressions in order to obtain the transmission coefficient to be used in Eqs. (2) and (3), the  $\Theta_\alpha^\pm$  matrices may be dropped, since they only provide a phase factor. The scattering matrix in the *channels* basis can then be written as

$$\bar{\mathcal{S}}^- = (U_s^-)^{-1} T_{sr} \mathcal{G}_{ra} S_{at} (\mathcal{G}_{tt}^0)^{-1} U_t^-. \quad (39)$$

For the opposite case, transmission from substrate to tip, we obtain

$$\bar{\mathcal{S}}^+ = (U_t^+)^{-1} T_{ta} \mathcal{G}_{ar} S_{rs} (\mathcal{G}_{ss}^0)^{-1} U_s^+. \quad (40)$$

### C. A simple model

Since for 1D symmetric junctions and in the zero-bias limit both the ESQC and the Green-function method just

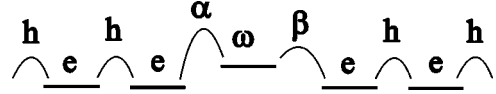


FIG. 3. Schematic of the simple 1D linear chain with one orbital per PL, and an impurity inserted at the interface.

developed provide an exact way of calculating the elastic-scattering transmission coefficient  $\mathcal{T}^\pm(E)$  (as long as we maintain the one-electron Hamiltonian), we wish to show their equivalence here. Rather than performing a rigorous proof, we choose the simple system depicted in Fig. 3, and which was already studied in Ref. 3. It consists of an infinite bulk chain into which an impurity has been inserted. The bulk chain contains just one orbital per PL, and we use a nearest-neighbor Hamiltonian characterized by the on-site energies  $e$  and the hopping interaction  $h$ . The energy at the impurity is  $\omega$  and its coupling to the chain is given by the interactions  $\alpha$  and  $\beta$ . We further assume that the AO basis is orthogonal, so that all overlaps between different PL's are zero.

If we identify the impurity with the block  $r$ , and the PL to its right with the tip apex  $a$ , we have  $F_{sr} = F_{rs} = \alpha$ ,  $F_{ar} = F_{ra} = \beta$ ,  $F_{rr} = E - \omega$ ,  $F_{ss} = F_{tt} = F_{aa} = E - e$ , and  $F_{ss\pm 1} = F_{tt\pm 1} = F_{at} = F_{ta} = h$ . By substituting these values into expressions (A21), (A17), (A2), (A18), and (A14), we obtain

$$S_{rs} = -\alpha[(E - e) + ht]^{-1}, \quad (41)$$

$$T_{ta} = -h[(E - e) + ht]^{-1}, \quad (42)$$

$$(\mathcal{G}_{ss}^0)^{-1} = (E - e) + 2ht, \quad (43)$$

$$(\mathcal{G}_{aa}^0)^{-1} = (E - e) - h^2[(E - e) + ht]^{-1}, \quad (44)$$

$$(\mathcal{G}_{rr}^0)^{-1} = (E - \omega) - \alpha^2[(E - e) + ht]^{-1}, \quad (45)$$

where  $t$  stands for the bulk transfer matrix:  $t = T_{s\pm 1s} = T_{t\pm 1t}$ . To obtain its value, we note that in this model  $a$  coincides with any PL at  $t$ , and therefore,  $T_{ta} = T_{t\pm 1t} = t$ . Then, by equating the expression for  $T_{ta}$  in Eq. (42) with  $t$ , we find

$$t = \frac{-(E - e)}{2h} \pm \frac{\sqrt{(E - e)^2 - 4h^2}}{2h}. \quad (46)$$

When  $E$  is contained in the interval  $e \pm 2h$  then  $t$  is imaginary with  $|t| = 1$  and we have a propagative channel in the chain. The set of parameters  $(e, h, \omega, \alpha, \beta)$  can be further reduced to four by defining  $q = (E - e)/h$ ,  $X = (\omega - e)/h$ ,  $Y = \alpha/h$ , and  $Z = \beta/\alpha$ . By substituting the above relations into Eq. (40) we may obtain an analytical expression for the transmission coefficient as a function of these new variables. The algebra involved is presented in Appendix B, and the final result is

$$\mathcal{T}(E) = \mathcal{T}_1 \mathcal{T}_2(E), \quad (47)$$

where

$$\mathcal{T}_1 = 4(Z + 1/Z)^{-2}, \quad (48)$$

$$\mathcal{T}_2(E) = \left( 1 + \frac{[X + q(W^2 - 1)]^2}{W^4(4 - q^2)} \right)^{-1}, \quad (49)$$

$$W = Y\sqrt{(1 + Z^2)/2}. \quad (50)$$

This result is identical to expressions (15) in Ref. 3. Notice that the use of Eq. (39) instead of Eq. (40) gives the same result, since we are considering the zero-bias limit.

This expression may be further simplified if we assume the limit  $\beta \ll \alpha$ . This approximation implies a weak interaction between the sample surface  $r$  and the tip apex  $a$ , which is the typical situation in the STM experiments. In this case,  $Z \ll 1$ ,  $\mathcal{T}_1 \approx 4Z^2$ , and  $W \approx Y/\sqrt{2}$ , and  $\mathcal{T}(E)$  may be expressed as

$$\mathcal{T}(E) \approx \frac{Z^2 Y^4 (4 - q^2)}{q^2(1 - Y^2) + Xq(Y^2 - 2) + X^2 + Y^4}. \quad (51)$$

On the other hand, the local density of states at  $r$  and  $a$  ( $\rho_r^0$  and  $\rho_a^0$ ) may be obtained from Eqs. (A22), (A23), and (41)–(45):

$$\rho_r^0 = \frac{1}{2\pi} \frac{Y^2 \sqrt{4 - q^2}}{h[q^2(1 - Y^2) + Xq(Y^2 - 2) + X^2 + Y^4]},$$

$$\rho_a^0 = \frac{2}{\pi} \frac{\sqrt{4 - q^2}}{h}, \quad (52)$$

and it is then easy to show that

$$\mathcal{T}(E) \propto \beta^2 \rho_a^0 \rho_r^0, \quad (53)$$

so that in the limit of a weak  $ar$  interaction,  $\beta \ll 1$ , we retrieve the Fermi golden rule. We stress, however, that such a simple relation is by no means an accurate approach to the real STM experiment. Any real surface being probed is far from the 1D idealization we have assumed in this section, and, when considering 3D interfaces, or even just allowing for a greater number of AO's at each layer, the appearance of interference effects<sup>9,14,15,17</sup> invalidates Eq. (53).

#### IV. 3D CASE

In this section we model the STM geometry in a more realistic way. The system is still divided into the same four blocks used for the 1D case,  $s$ ,  $r$ ,  $a$ , and  $t$ , but PL's are now assumed to be composed of atomic planes which are periodic in the lateral direction. Within the bulk materials  $s$  or  $t$ , all atomic planes are parallel to each other and have the same in-plane lattice vectors  $\vec{\rho}_s$  or  $\vec{\rho}_t$ . The propagation direction at each wire coincides with the repeat vector linking adjacent PL's in the bulk material. Obviously, the atomic planes cannot contain the propagation direction. The lattices at the surface blocks  $\vec{\rho}_r$  or  $\vec{\rho}_a$  are further assumed to be commensurate with their respective bulk lattices  $\vec{\rho}_s$  or  $\vec{\rho}_t$ , respectively. Although the tip apex block  $a$  is not periodic in the real STM experiment, we will assume it as such for now, and show below how we can accurately retrieve the nonperiodic limit. The model is schematically shown in Fig. 1(d). It is important to realize that the geometrical descriptions of the wires are uncorrelated. This means that the lattices at  $rs$  will be in

general incommensurate with those at  $at$ . Furthermore, neither the propagation direction nor the orientation of the atomic planes at one wire have to be aligned with those at the other wire.

We can then form at each PL  $n$  a set of 2D Bloch waves, each one corresponding to a different wave vector  $\vec{k}_\alpha$  contained in the 2D Brillouin zone (BZ) of the layer.<sup>20</sup> We follow the notation of Sec. III, so that  $\alpha$  stands for  $s$  if  $n < -1$ ,  $r$  if  $n = -1$ ,  $a$  if  $n = 1$  or  $t$  if  $n > 1$ . In analogy with Eq. (6), we denote the 2D Bloch wave-function amplitudes at PL  $n$  by  $|a_n(\vec{k}_\alpha)\rangle$ :

$$|a_n(\vec{k}_\alpha)\rangle = \sum_{i=1}^{N_\alpha} a_{i,n}(\vec{k}_\alpha) |\alpha_i(\vec{d}_n, \vec{k}_\alpha)\rangle. \quad (54)$$

Here,  $|\alpha_i(\vec{d}_n, \vec{k}_\alpha)\rangle$  gives the Bloch state  $\vec{k}_\alpha$  of orbital  $\alpha_i$  in layer  $n$ :

$$|\alpha_i(\vec{d}_n, \vec{k}_\alpha)\rangle = \frac{1}{\sqrt{N_{\vec{\rho}_\alpha}}} \sum_{\vec{\rho}_\alpha} e^{i\vec{k}_\alpha \vec{\rho}_\alpha} |\alpha_i(\vec{\rho} + \vec{d}_n)\rangle, \quad (55)$$

where  $N_{\vec{\rho}_\alpha}$  is the number of lattice points in the layer (see below).

The  $F$  matrices given in Eq. (17) must also be modified to include the  $\vec{k}_\alpha$  dependence. For a diagonal matrix block  $nn$  we use the notation  $F_{nn}(\vec{k}_\alpha)$ , whose elements are given by

$$\langle \alpha_i | F_{nn}(\vec{k}_\alpha) | \alpha_j \rangle = \langle \alpha_i(\vec{d}_n, \vec{k}_\alpha) | F | \alpha_j(\vec{d}_n, \vec{k}_\alpha) \rangle, \quad (56)$$

while for the off-diagonal matrix blocks  $nn'$  we use  $F_{nn'}(\vec{k}_\alpha, \vec{k}'_\alpha)$  with elements

$$\langle \alpha_i | F_{nn'}(\vec{k}_\alpha, \vec{k}'_\alpha) | \alpha'_j \rangle = \langle \alpha_i(\vec{d}_n, \vec{k}_\alpha) | F | \alpha'_j(\vec{d}_{n'}, \vec{k}'_\alpha) \rangle. \quad (57)$$

Due to translation symmetry, all matrix blocks  $F_{nn'}(\vec{k}_\alpha, \vec{k}'_\alpha)$  that relate PL's  $n$  and  $n'$  located in the same block  $\alpha$  are zero if  $\vec{k}_\alpha \neq \vec{k}'_\alpha$ . Therefore, in the  $s$  and  $t$  bulk regions the 2D Bloch functions do not mix between each other, and we may regard each  $\vec{k}_\alpha$  state as an independent 1D linear chain.<sup>20</sup> This decoupling allows us to retain the Landauer-Büttiker picture of independent channels in the wires and, expressions (2) and (3) for the current can be generalized by noting that the  $\vec{k}_\alpha$  index acts just as another quantum number:

$$I(V) = \frac{e}{\pi\hbar} \int_0^{-eV} dE \sum_{\vec{k}'_\alpha, \vec{k}_\alpha} \sum_{mm'} \mathcal{T}_{m',m}^\pm(\vec{k}'_\alpha, \vec{k}_\alpha, E + \mu_s), \quad (58)$$

where the transmission probability matrix is now given by

$$\mathcal{T}_{m',m}^\pm(\vec{k}'_\alpha, \vec{k}_\alpha) = |\bar{\mathcal{S}}_{m',m}^\pm(\vec{k}'_\alpha, \vec{k}_\alpha)|^2 \frac{v_{\alpha'}^{m'}(\vec{k}'_\alpha)}{v_\alpha^m(\vec{k}_\alpha)}. \quad (59)$$

As in the 1D case, the problem again reduces to obtaining the scattering matrix  $\bar{\mathcal{S}}^\pm$  in the Bloch basis,

$$\bar{\mathcal{S}}_{m',m}^\pm(\vec{k}'_\alpha, \vec{k}_\alpha) = \langle u_{n'}^{\pm m'}(\vec{k}'_\alpha) | \mathcal{S}^\pm | u_n^{\pm m}(\vec{k}_\alpha) \rangle, \quad (60)$$

for which we may still use relations (39) and (40), but the explicit expressions for the matrices involved need revision.

First, bulk quantities may be evaluated in the same way as in Sec. III by simply replacing the  $F$  matrix elements of Eq. (17) with the above expressions (56) and (57). In particular, the band structure  $\Theta_\alpha^\pm(\vec{k}_\alpha)$  and the corresponding eigenvector matrix  $U_\alpha^\pm(\vec{k}_\alpha)$  at each  $\vec{k}_\alpha$  can be found via the eigenvalue problem (36):

$$T_{\alpha\pm 1\alpha}(\vec{k}_\alpha)U_\alpha^\pm(\vec{k}_\alpha) = U_\alpha^\pm(\vec{k}_\alpha)\Theta_\alpha^\pm(\vec{k}_\alpha), \quad (61)$$

where the  $T_{\alpha\pm 1\alpha}(\vec{k}_\alpha)$  transfer matrices are evaluated in the same way as for the 1D case using expressions (A3)–(A8). The diagonal blocks of the bulk Green functions  $\mathcal{G}_{ss}^\pm(\vec{k}_s)$  or  $\mathcal{G}_{tt}^\pm(\vec{k}_t)$  are then easily obtained via Eq. (A2).

The next task is to include the effect of the surface on each of the bulk blocks. Let us first consider the  $rs$  case. We assume the lattice  $\vec{\rho}_r$  at PL  $r$  to be commensurate with the bulk lattice  $\vec{\rho}_s$ ,  $M_{\vec{G}_{rs}}$  being the ratio between the sizes of both unit cells. In this case, each surface  $\mathbf{k}$  vector  $\vec{k}_r$  will only couple to the bulk  $\vec{k}_r + \vec{G}_{rs}$  chains, where  $\vec{G}_{rs}$  are the  $M_{\vec{G}_{rs}}$  surface reciprocal lattice vectors contained in the bulk BZ. Therefore, to find the surface Green function  $\mathcal{G}_{rr}^0(\vec{k}_r)$ , we may still use Eq. (A14), but including a summation over  $\vec{G}_{rs}$ :

$$I = \left\{ \left( \sum_{\vec{G}_{rs}}^{M_{\vec{G}_{rs}}} F_{rs}(\vec{k}_r, \vec{k}_r + \vec{G}_{rs}) T_{sr}(\vec{k}_r + \vec{G}_{rs}, \vec{k}_r) \right) + F_{rr}(\vec{k}_r) \right\} \mathcal{G}_{rr}^0(\vec{k}_r), \quad (62)$$

whereas the  $T_{sr}(\vec{k}_r + \vec{G}_{rs}, \vec{k}_r)$  transfer matrix is obtained from Eq. (A17),

$$T_{sr}(\vec{k}_r + \vec{G}_{rs}, \vec{k}_r) = -\{F_{ss}(\vec{k}_r + \vec{G}_{rs}) + F_{ss-1}(\vec{k}_r + \vec{G}_{rs}) \times T_{s-1s}(\vec{k}_r + \vec{G}_{rs})\}^{-1} F_{sr}(\vec{k}_r + \vec{G}_{rs}, \vec{k}_r), \quad (63)$$

and a related expression for the other transfer matrix  $S_{rs}(\vec{k}_r, \vec{k}_r + \vec{G}_{rs})$  can be obtained by using Eq. (A21):

$$S_{rs}(\vec{k}_r + \vec{G}_{rs}, \vec{k}_r) = -F_{rs}(\vec{k}_r, \vec{k}_r + \vec{G}_{rs}) \{F_{ss}(\vec{k}_r + \vec{G}_{rs}) + F_{ss-1}(\vec{k}_r + \vec{G}_{rs}) T_{s-1s}(\vec{k}_r + \vec{G}_{rs})\}^{-1}. \quad (64)$$

Similar reasonings can be applied to the  $at$  blocks. In this case, however, the tip apex is not periodic, and we wish to keep the AO basis set for this block instead of the 2D Bloch wave representation. To this end, the BZ at  $a$  should be shrunk to a point, but this generates normalization problems. We overcome this difficulty by assuming that the tip apex is actually periodic. The corresponding lattice  $\vec{\rho}_a$  is chosen such that it is commensurate with that at the bulk block  $\vec{\rho}_t$ , and the ratio of their unit cell sizes  $M_{\vec{G}_{at}}$  is much greater than unity. This yields a very small BZ at  $a$ , so that we may

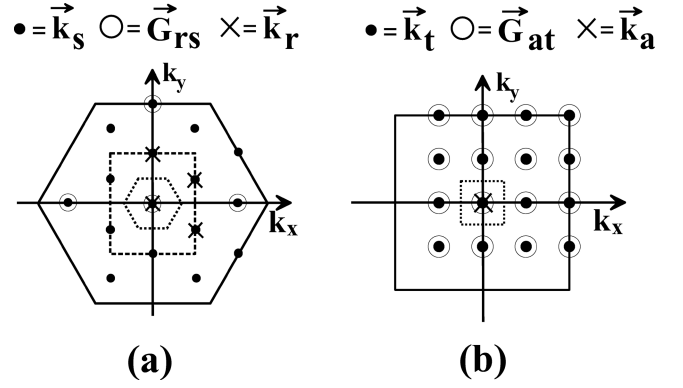


FIG. 4.  $\mathbf{k}$ -space sampling (solid dots) at each bulk block. Open circles indicate the surface reciprocal-lattice points, while crosses give the resulting surface  $\mathbf{k}$  mesh. The bulk, surface, and  $\mathbf{k}$ -supercell 2D BZ's are indicated by solid, dashed, and dotted lines, respectively; (a)  $rs$  block assuming an hexagonal lattice for  $s$  and a rectangular  $c(4 \times 2)$  lattice for  $r$ ; and (b)  $at$  block, with a square lattice for both  $a$  and  $t$ . The 2D BZ at  $a$  is not shown, since it is coincident with the  $\mathbf{k}$ -supercell BZ. In both cases the  $\mathbf{k}$  supercell corresponds to a  $p(4 \times 4)$  lattice.

neglect all  $\vec{k}_a$  vectors at this PL except  $\vec{k}_a = \vec{0}$ , which will couple to all the bulk  $\vec{G}_{at}$  chains, where  $\vec{G}_{at}$  are the  $M_{\vec{G}_{at}}$  surface reciprocal-lattice vectors at  $a$  contained in the bulk BZ of the  $t$  block. Consequently, the expressions for  $\mathcal{G}_{aa}^0(\vec{0}_a)$ ,  $T_{ta}(\vec{G}_{at}, \vec{0}_a)$ , and  $S_{at}(\vec{0}_a, \vec{G}_{at})$  are analogous to Eqs. (62)–(64) derived for the  $rs$  blocks. Clearly, in the limit of  $M_{\vec{G}_{at}}$  very large, the localized AO basis set picture at  $a$  is recovered.

As for the choice of the  $\vec{k}_\alpha$  vectors summed up in Eq. (58), we must first realize that even if the isolated  $rs$  and  $at$  wires possess a certain 2D symmetry in real space; when combining both to form the whole of the STM system, and allowing for tip displacements relative to the substrate, any symmetry will be lost. This lack of symmetry impedes the use of efficient  $\mathbf{k}$ -sampling schemes.<sup>27</sup> Instead, we assume that PL's at each wire can be described by a large supercell, denoted by the  $\mathbf{k}$  supercell, which is commensurate with both the surface and bulk lattices at that wire, and we apply the usual periodic boundary conditions. Accordingly, if the  $\mathbf{k}$  supercell contains  $N_{\vec{\rho}_\alpha}$  bulk unit cells, we then obtain a set of  $N_{\vec{k}_\alpha}$  allowed  $\mathbf{k}$  points at each bulk block  $\alpha$ , where  $N_{\vec{k}_\alpha} = N_{\vec{\rho}_\alpha}$ .

For the  $rs$  chain, the resulting  $\vec{k}_s$  grid will determine at the same time the  $N_{\vec{k}_r}$  allowed surface wave vectors at  $r$ , where  $N_{\vec{k}_r} = N_{\vec{k}_s} / N_{\vec{G}_{rs}}$ . These  $\vec{k}_r$  vectors correspond simply to those  $\vec{k}_s$  which lie inside the surface BZ, whereas if  $\vec{k}_s$  falls outside, then it will be related to a particular  $\vec{k}_r$  by addition of a surface reciprocal lattice vector  $\vec{G}_{rs}$ . An example of this  $\mathbf{k}$  sampling procedure is shown in Fig. 4(a).

Similarly, the choice of the  $\vec{k}_t$  wave vectors at  $t$  may be done by defining another large  $\mathbf{k}$  supercell commensurate with  $\vec{\rho}_t$  and  $\vec{\rho}_a$ . In fact, it is convenient to choose the  $\mathbf{k}$  supercell coincident with the lattice  $\vec{\rho}_a$  imposed at the apex block  $a$ . We then have  $N_{\vec{\rho}_t} = N_{\vec{k}_t} = N_{\vec{G}_{at}}$  and all  $\vec{k}_t$  coincide with the reciprocal-lattice vectors  $\vec{G}_{at}$  contained in the BZ at

$t$ . Obviously, since we only have the  $\vec{0}_a$  vector at  $a$ ,  $N_{\vec{k}_a} = N_{\vec{p}_a} = 1$ . An example for this case is provided in Fig. 4(b).

Finally, we need to evaluate the 3D interface Green function  $\mathcal{G}_{II}$  by applying the SGFM method. The lattice  $\vec{\rho}_r$  at  $r$  will not in general be commensurate with that imposed at  $a$ ,  $\vec{\rho}_a$ . This implies that the tip apex  $a$  can couple different  $\vec{k}_r$  vectors, and the states  $|a_r(\vec{k}_r)\rangle$  can no longer be treated as independent when the block  $a$  is present. The Green function matrix blocks  $\mathcal{G}_{rr}(\vec{k}_r, \vec{k}'_r)$  are then nonzero, as opposed to the isolated surface. Therefore, when calculating  $\mathcal{G}_{II}$  through Eq. (20), all  $\mathcal{G}_{rr}(\vec{k}_r, \vec{k}'_r)$  blocks should be computed at the same time. The matrix to be inverted appearing in the third term of Eq. (20) must then include all  $(\vec{k}_r, \vec{k}'_r)$  blocks and its dimensions can become rather large [ $\approx (10^3 \times 10^3)$ ]. Thus an exact calculation of  $\mathcal{G}_{II}$  becomes too time consuming to render the method efficient. Instead, we approximate the evaluation of the  $\mathcal{G}_{ra}(\vec{k}_r, \vec{0}_a)$  blocks by assuming that  $a$  does not actually couple states at  $r$  with different  $\vec{k}_r$ . Under this assumption, Eq. (20) reads

$$\begin{aligned} \mathcal{G}_{II}(\vec{k}_r, \vec{0}_a) &= \begin{pmatrix} \mathcal{G}_{rr}(\vec{k}_r, \vec{k}_r) & \mathcal{G}_{ra}(\vec{k}_r, \vec{0}_a) \\ \mathcal{G}_{ar}(\vec{0}_a, \vec{k}_r) & \mathcal{G}_{aa}(\vec{0}_a, \vec{0}_a) \end{pmatrix} \\ &\approx \begin{pmatrix} [\mathcal{G}_{rr}^0(\vec{k}_r, \vec{k}_r)]^{-1} & F_{ra}(\vec{k}_r, \vec{0}_a) \\ F_{ar}(\vec{0}_a, \vec{k}_r) & [\mathcal{G}_{aa}^0(\vec{0}_a, \vec{0}_a)]^{-1} \end{pmatrix}^{-1}. \end{aligned} \quad (65)$$

Test calculations comparing Eq. (65) with its exact version proved the approximation to be excellent for any realistic tip-sample distance  $z$ . For instance, the transmission coefficient is affected by less than 1% when  $z$  is only 4 Å. This is an expected result, since to collect an electron at  $a$  which has changed its wave vector at  $r$  from  $\vec{k}_r$  to  $\vec{k}'_r$ , it must first tunnel to  $a$  where it loses the parallel momentum, then tunnel back to  $r$  picking up the  $\vec{k}'_r$  vector and finally transmit again to  $a$ . Therefore, the contribution to the transmission arising from the  $\mathcal{G}_{rr}(\vec{k}_r, \vec{k}'_r)$  terms involves at least three tunneling processes, and becomes negligible when typical transmission amplitudes across the junction are used.

To summarize, our final general expressions for the scattering matrices in the 3D case are therefore

$$\begin{aligned} \bar{S}^-(\vec{k}_s, \vec{k}_t) &= [U_s^-(\vec{k}_s)]^{-1} T_{sr}(\vec{k}_s, \vec{k}_r) \mathcal{G}_{ra}(\vec{k}_r, \vec{0}_a) S_{at}(\vec{0}_a, \vec{k}_t) \\ &\quad \times [\mathcal{G}_{tt}^0(\vec{k}_t)]^{-1} U_t^-(\vec{k}_t), \end{aligned} \quad (66)$$

$$\begin{aligned} \bar{S}^+(\vec{k}_t, \vec{k}_s) &= [U_t^+(\vec{k}_t)]^{-1} T_{ta}(\vec{k}_t, \vec{0}_a) \mathcal{G}_{ar}(\vec{0}_a, \vec{k}_r) S_{rs}(\vec{k}_r, \vec{k}_s) \\ &\quad \times [\mathcal{G}_{ss}^0(\vec{k}_s)]^{-1} U_s^+(\vec{k}_s), \end{aligned} \quad (67)$$

where  $\vec{k}_s = \vec{k}_r + \vec{G}_{rs}$  and  $\vec{k}_t = \vec{G}_{at}$ .

We may further simplify the structure of  $\bar{S}^\pm$  by defining the renormalized transfer matrices  $\bar{T}_{\alpha\alpha'}$  as

$$\bar{T}_{sr}(\vec{k}_s, \vec{k}_r) = [U_s^-(\vec{k}_s)]^{-1} T_{sr}(\vec{k}_s, \vec{k}_r), \quad (68)$$

$$\bar{T}_{at}(\vec{0}_a, \vec{k}_t) = S_{at}(\vec{0}_a, \vec{k}_t) [\mathcal{G}_{tt}^0(\vec{k}_t)]^{-1} U_t^-(\vec{k}_t), \quad (69)$$

$$\bar{T}_{ta}(\vec{k}_t, \vec{0}_a) = [U_t^+(\vec{k}_t)]^{-1} T_{ta}(\vec{k}_t, \vec{0}_a), \quad (70)$$

$$\bar{T}_{rs}(\vec{k}_r, \vec{k}_s) = S_{rs}(\vec{k}_r, \vec{k}_s) [\mathcal{G}_{ss}^0(\vec{k}_s)]^{-1} U_s^+(\vec{k}_s), \quad (71)$$

so that we arrive at the compact expressions

$$\bar{S}^-(\vec{k}_s, \vec{k}_t) = \bar{T}_{sr}(\vec{k}_s, \vec{k}_r) \mathcal{G}_{ra}(\vec{k}_r, \vec{0}_a) \bar{T}_{at}(\vec{0}_a, \vec{k}_t), \quad (72)$$

$$\bar{S}^+(\vec{k}_t, \vec{k}_s) = \bar{T}_{ta}(\vec{k}_t, \vec{0}_a) \mathcal{G}_{ar}(\vec{0}_a, \vec{k}_r) \bar{T}_{rs}(\vec{k}_r, \vec{k}_s). \quad (73)$$

Relations (72) and (73) have a simple physical interpretation. The  $\bar{T}_{\alpha\alpha'}$  matrices linking the bulk blocks  $s$  and  $t$  to their respective surfaces  $r$  and  $a$  account for all the multiple scattering events between the bulk channels and the orbitals at each surface. On the other hand, the Green-function matrices  $\mathcal{G}_{ra}$  and  $\mathcal{G}_{ar}$  relate the wave amplitudes at  $r$  and  $a$  and, again, they include both the intralayer multiple scattering at  $r$  and  $a$  as well as the interlayer multiple scattering between  $r$  and  $a$ .

It is also clear that these expressions become computationally very suited for evaluating entire STM images since the  $\bar{T}_{\alpha\alpha'}$  matrices only depend on the unperturbed system (i.e., the isolated wires). Therefore, one may first evaluate these matrices for all energies and  $\mathbf{k}$  vectors. Next, for each tip position relative to the sample origin we only need to reevaluate the  $F_{ar}$  and  $F_{ra}$  matrices in the secular equation of the entire system, and solve Eq. (65) for the Green-function matrix block  $\mathcal{G}_{ar}$  or  $\mathcal{G}_{ra}$  depending on the bias sign. The scattering matrix elements are then computed by simple matrix multiplications and the current is obtained directly through Eqs. (58) and (59).

### Current analysis

One of the major aims of the present theory is the possibility to provide an easy interpretation to the origin of the contrast in the final STM image. Generally speaking, one wishes to identify which AO's or which interactions at the interface dominate this contrast, and how their contributions to the current are modified as the tip is displaced across the sample surface. However, and as can be seen from Eqs. (72), (73), (58), and (59), the entire electron transmission process is a rather complex one, involving both multiple-scattering events and interference effects; an electron propagating along a certain ingoing channel is scattered at the interface, and its wave field, after considering all the scattering paths, will be distributed among the AO's at the interface. The associated probability for the electron to end up in a certain outgoing channel at the opposite wire will depend on the net interference among all these scattering paths. Unfortunately, the SGFM, by evaluating the  $\mathcal{G}_{ar}$  or  $\mathcal{G}_{ra}$  matrices at one stroke through the inversion of Eq. (65), hinders the possibility of separating the intralayer from the interlayer multiple scattering at the interface or, in other words, it carries too many scattering events to permit a comprehensible analysis of which  $a$ - $r$  interactions contributed most to the final current.

A simple way out of this problem is to obtain the Green function of the entire system  $\mathcal{G}$ , by expanding the Dyson equation in the following way:

$$\mathcal{G} = \mathcal{G}^0 + \mathcal{G}^0 \Delta F \mathcal{G} \approx \mathcal{G}^0 + \mathcal{G}^0 \Delta F \mathcal{G}^0 + \mathcal{G}^0 \Delta F \mathcal{G}^0 \Delta F \mathcal{G}^0 + \dots \quad (74)$$

By noting that the unperturbed system corresponds to the isolated wires, it is then trivial to show that the interface matrix blocks  $\mathcal{G}_{ar}^1$  and  $\mathcal{G}_{ra}^1$ , up to first order in Eq. (74), are given by

$$\mathcal{G}_{ar}^1 = \mathcal{G}_{aa}^0 F_{ar} \mathcal{G}_{rr}^0, \quad \mathcal{G}_{ra}^1 = \mathcal{G}_{rr}^0 F_{ra} \mathcal{G}_{aa}^0. \quad (75)$$

Thus these expressions decouple the intralayer scattering at each surface (matrices  $\mathcal{G}_{aa}^0$  and  $\mathcal{G}_{rr}^0$ ) at the cost of considering just one tunneling event ( $F_{ar}$  or  $F_{ra}$ ) across the junction. Nevertheless, this approximation is usually very accurate since the tunneling matrix elements of  $F_{ar}$  or  $F_{ra}$  are small for typical tip sample distances used in the STM experiment, implying that the  $r$ - $a$  interlayer multiple scattering hardly affects the final current value. In fact, several STM theories have successfully relied on this approximation.<sup>2</sup>

Upon substituting Eq. (75) into Eqs. (72) and (73), we may define the first-order scattering matrix  $\mathcal{S}^{1\pm}$  as

$$\bar{\mathcal{S}}^{-}(\vec{k}_s, \vec{k}_t) = \bar{T}_{sr}(\vec{k}_s, \vec{k}_r) \mathcal{G}_{ra}^1(\vec{k}_r, \vec{0}_a) \bar{T}_{at}(\vec{0}_a, \vec{k}_t), \quad (76)$$

$$\bar{\mathcal{S}}^{+}(\vec{k}_t, \vec{k}_s) = \bar{T}_{ta}(\vec{k}_t, \vec{0}_a) \mathcal{G}_{ar}^1(\vec{0}_a, \vec{k}_r) \bar{T}_{rs}(\vec{k}_r, \vec{k}_s), \quad (77)$$

while the total transmission coefficient up to first order,  $\mathcal{T}^{1\pm}$ , may be written as

$$\mathcal{T}^{1\pm} = \sum_{m\alpha, m'\alpha'} |\bar{\mathcal{S}}^{1\pm}(m\alpha, m'\alpha')|^2, \quad (78)$$

where now the  $m\alpha$  index stands for both the band index and the  $\vec{k}_\alpha$  vector, and we have further assumed that the group velocities  $v_\alpha^m$  appearing in Eq. (59) are already included in the renormalized transfer matrices  $\bar{T}_{\alpha\alpha'}$ . The energy dependence has also been omitted, but it must be recalled that  $\mathcal{T}^{1\pm}$  is evaluated in Eq. (78) for a particular energy value  $E$ .

The total first-order transmission coefficient may be decomposed into the interference matrix terms  $\mathcal{T}_{\alpha\alpha'}^{1\pm}(\alpha_i - \alpha'_j, \alpha_{i'} - \alpha'_{j'})$  between the  $(\alpha_i - \alpha'_j)$  and  $(\alpha_{i'} - \alpha'_{j'})$  interactions, where  $\alpha$  and  $\alpha'$  stand for  $r$  or  $a$ . Under a negative sample bias, these terms are given by

$$\begin{aligned} & \mathcal{I}^{-}(r_i - a_j, r_{i'} - a_{j'}) \\ &= \sum_{ms, m't} \{ [\bar{T}_{ta} G_{aa}^0](m't, a_j) F(m't, a_j, ms, r_i) \\ & \quad \times [G_{rr}^0 \bar{T}_{rs}](ms, r_i) \} \times \{ [\bar{T}_{ta} G_{aa}^0](m't, a_{j'}) \\ & \quad \times F(m't, a_{j'}, ms, r_{i'}) [G_{rr}^0 \bar{T}_{rs}](ms, r_{i'}) \}^*, \end{aligned} \quad (79)$$

and a similar expression for the positive bias case. Here we use  $[AB](i, j)$  to denote the  $(i, j)$  element of the matrix product  $AB$  and the \* superscript stands for the complex conjugate.

The diagonal terms in Eq. (79),  $\mathcal{I}^{-}(r_i - a_j, r_i - a_j)$ , give the contribution to the total probability arising from an electron which has tunneled from  $a_j$  to  $r_i$  in the absence of any interference with the rest of tunneling paths. The off-diagonal elements correspond, on the other hand, to the contribution arising solely from the interference between the  $(r_i - a_j)$  and  $(r_{i'} - a_{j'})$  interactions and hence, they might be positive or negative, in which case the interference will be constructive or destructive, respectively.

From the interference matrix we may define the  $\mathcal{T}_{ra}^{1\pm}(r_i, a_j)$  quantities as

$$\mathcal{T}_{ra}^{1\pm}(r_i, a_j) = \sum_{r_i', a_j'}^{N_r, N_a} \mathcal{I}^{-}(r_i - a_j, r_{i'} - a_{j'}), \quad (80)$$

giving the contribution to  $\mathcal{T}^{1\pm}$  arising from an electron which has tunneled from  $r_i$  to  $a_j$  (or vice versa if the bias is positive), after the interference with the rest of the tunneling paths has been taken into account.

A more general view of how the current is distributed among the orbitals at the interface may be achieved through the individual AO components  $\mathcal{T}_\alpha^{1\pm}(\alpha_i)$  of the first-order transmission coefficient:

$$\mathcal{T}_r^{1\pm}(r_i) = \sum_{a_j}^{N_a} \mathcal{T}_{ra}^{1\pm}(r_i, a_j), \quad \mathcal{T}_a^{1\pm}(a_j) = \sum_{r_i}^{N_r} \mathcal{T}_{ra}^{1\pm}(r_i, a_j), \quad (81)$$

so that the sum of the individual components at any of the two surface blocks,  $\alpha = r$  and  $a$ , adds up to the total transmission

$$\begin{aligned} \mathcal{T}^{1\pm} &= \sum_{\alpha_i}^{N_\alpha} \mathcal{T}_\alpha^{1\pm}(\alpha_i) = \sum_{r_i, a_j}^{N_r, N_a} \mathcal{T}_{ra}^{1\pm}(r_i, a_j) \\ &= \sum_{r_i, a_j}^{N_r, N_a} \sum_{r_i', a_j'}^{N_r, N_a} \mathcal{I}^{\pm}(r_i - a_j, r_{i'} - a_{j'}). \end{aligned} \quad (82)$$

Therefore, an inspection of the  $\mathcal{T}_r^{1\pm}(r_i)$  values already provides valuable information on which surface AO's are being imaged (i.e., contribute most to the total current), while from the  $\mathcal{T}_a^{1\pm}(a_j)$  quantities one can deduce which tip states act as the main probing orbitals. We must also recall that any component  $\mathcal{T}_\alpha^{1\pm}(\alpha_i)$  may attain negative values if the interference terms involving this orbital result in a net destructive interference.

## V. INELASTIC EFFECTS

So far, we have developed the formalism of Secs. III and IV under the elastic scattering limit used by Büttiker *et al.* to deduce their multichannel formula for transmission, Eqs. (2) and (3). Under this assumption, any electron energy loss is neglected, and the electron flux is conserved. It should be noted, however, that in using approximation (1) for the evaluation of the current, we are not strictly neglecting inelastic scattering effects, and we may in fact include a certain amount of damping during the electron propagation from one reservoir to the other. To this end, we add an imaginary component to the real energy  $E_r$  at which the *elastic* transmission probability  $\mathcal{T}_{mm'}^{\pm}(E_r)$  is to be evaluated, which acts

as an optical potential just as in low-energy electron-diffraction theory.<sup>28</sup> This approach suits naturally the Green-function formalism, as it suffices to set  $\delta$  in Eq. (16) to any desired value of the optical potential, leaving the rest of the equations derived above unchanged. Similar modelings of the inelastic effects in related problems have been used by different authors.<sup>29</sup>

If we assume relaxation times for the conducting electrons of the order of  $\sim 10^{-13}$ – $10^{-14}$  s, then the corresponding linewidths are  $\sim 0.01$ – $0.1$  eV, and we may set the optical potential in the bulk blocks  $\delta_\alpha$  ( $\alpha=s$  or  $t$ ) to these values. As regards inelastic effects at the surfaces  $r$  and  $a$ , one expects smaller relaxation times for these blocks than for the bulk and, accordingly, we may set  $\delta$  at these blocks to an upper limit of  $\delta_a = \delta_r = 0.1$  eV.

However, the inclusion of damping into the formalism generates some ambiguity when defining the propagative channels, since now the  $\theta_\alpha^m(E)$  wave numbers in Eqs. (10) and (11) all become complex quantities, and the distinction between propagating and evanescent waves is not clear any more. In principle, it is easy to expand  $\theta_\alpha^m(E)$  analytically to first order to obtain an approximate value of the wave number at real energy  $E_r$ :

$$\theta_\alpha^m(E_r) \approx \theta_\alpha^m(E) - i \delta_\alpha \frac{\partial \theta_\alpha^m}{\partial E} = \theta_\alpha^m(E) - \frac{i \delta_\alpha}{v_\alpha^m}, \quad (83)$$

which allows us to discern whether  $\theta_\alpha^m$  at real energy is an evanescent or propagative wave. Relation (83) turns out to be a useful approximation for values of  $\delta_\alpha \leq 0.01$  eV. Nevertheless, when taking the limits  $|n|, |n'| \geq 2$  in Eqs. (12) and (13), any Bloch function with a wave number that contains a non-negligible imaginary part will suffer a considerable decay before reaching the interface or the opposite reservoir, regardless of whether it would be a nondispersive channel at real energy. Therefore, we believe that a meaningful criterion is to regard as propagative channels those for which  $|e^{i\theta}| > C$ , where  $C$  is a preselected decay cutoff, and then to evaluate the transmission matrix elements only for these channels according to expressions (66) and (67); i.e., dropping the  $\Theta$  matrices just as we did in Eq. (38) to obtain our final expressions (39) and (40) for  $\bar{S}^\pm(E)$  in the 1D case. For instance, if the optical potential is set to  $\delta_\alpha \sim 0.01$  eV, a cutoff value of  $C = 0.97$  gives good results.<sup>23</sup>

A related and important issue is the setup of an efficient scheme for the energy integration in Eq. (58). The energy step to be used in the numerical integration should not be larger than the imaginary part of the energy  $\delta_\alpha$  since, otherwise, one may skip resonant peaks in the transmission coefficient which could give the dominant contribution to the current. For small biases ( $V \leq 0.1$  V) a value of  $\delta_\alpha = 0.01$  eV is computationally still adequate, but when considering larger STM biases the number of energy points becomes too large and the calculations too expensive, so that  $\delta_\alpha$  has to be increased to values around  $0.05$ – $0.1$  eV. As a consequence, all the Bloch waves become essentially evanescent with  $|e^{i\theta}| < 0.95$ , so that the nearly elastic scattering assumption is not well satisfied. Nonetheless, by reducing  $C$  to  $0.93$ – $0.87$ , we can still select a considerable number of the propagating channels existing in the  $\delta_\alpha = 0.01$  eV ( $C = 0.97$ ) case and,

fortunately, for most systems, the shape and corrugation of the images are only weakly affected by the precise value of  $\delta_\alpha$ .<sup>23</sup> The main difference between a high or low value of the optical potential is the tip-sample separation  $z$ , since to achieve the same current value  $I(V)$  under a strong damping the tip must come closer to the substrate.

It is also worth mentioning that besides the elastic-scattering limit, a major approximation in the LBF is the neglect of any interference effects or contributions to the measured resistance arising from the coupling of the channels to the reservoirs. If this contribution is comparable to the gap resistance at the interface, this approximation can generate discrepancies when comparing measured and LBF calculated resistances,<sup>25</sup> and extreme experimental care is necessary to filter out the resistance arising from the scattering at the wire-reservoir junctions.<sup>12</sup> Fortunately, typical STM measurements are far from this problem, since essentially all the resistance arises from the electron tunneling through the potential barrier localized at the junction.

## VI. FINAL DISCUSSION

A fundamental issue prior to applying a given theory is to establish its overall accuracy and, consequently, we summarize here the most crucial approximations in our STM formalism. Let us first assume that the geometry of Fig. 1 chosen to model the STM is correct. We then have as the main sources of inaccuracy the  $\mathbf{k}$  sampling and the treatment of inelastic effects. For the former, we find that  $\mathbf{k}$  grids composed of  $200$ – $400$  points at each bulk block are already well converged, in the sense that the transmission coefficients are affected by less than  $\pm 10\%$  if one further increases the density of the  $\mathbf{k}$  grid. If the image is calculated in the topographic mode, this translates into tip height uncertainties of only  $\sim 0.02$  Å for typical gap resistances of  $100$  MΩ. The precise value of the optical potential  $\delta$ , on the other hand, has a much stronger influence on the tip height  $z$ , and induces errors up to  $0.5$  Å for the same gap resistance.<sup>23</sup> The reason is that as  $\delta$  is increased the damping also increases and the tunnel current decreases. Correspondingly, the  $z$  value (tip height) becomes smaller. However, and provided that one includes enough channels in the calculation, the effect of the damping on the calculated current  $I(V)$  is more or less independent of the  $x$ - $y$  position of the tip, so that all pixels in the STM image are basically affected in the same way. The implication is that the uncertainty on the corrugation is much smaller than the error in  $z$ . From the numerical point of view, the formalism generates uncertainties in the corrugation of around  $0.03$  Å, and the final shape of the image is therefore hardly modified by the  $\mathbf{k}$  sampling or the optical potential.<sup>23</sup> Thus, as long as we do not choose too unreasonable values for the density of the  $\mathbf{k}$  grid,  $\delta$  or  $C$ , the theory should still provide a reliable way of identifying the main features present in the STM image via a qualitative comparison with the experiment.

As regards the zero-temperature limit assumed for the entire formalism, we also do not believe that this can be a major cause of inaccuracy. Expressions (2) and (3) can be easily generalized to nonzero temperatures<sup>19</sup> by including the Fermi-Dirac distributions of the two wires and performing the energy integration over a wider range than the  $[0, -eV]$

interval used for the  $T=0$  case. However, the smearing out of sharp features in the electronic structure of the system via the use of an optical potential tends to minimize any possible effects arising from energies outside the  $[0, -eV]$  range. On the other hand, typical measured thermovoltages at the STM junction are only of the order of  $10^{-6}$  V.<sup>13</sup>

A more delicate issue is to estimate the errors introduced by the modeling of the inelastic effects via an optical potential or the neglect of electron-electron interactions. The existence of other more sophisticated approaches should be pointed out,<sup>9,30,31</sup> but they have been developed mainly in order to explain specific features in certain experiments, and this kind of study is far beyond the scope of our theory. As a matter of fact, it is most common in STM theories to neglect inelastic effects and still, the experiment-theory agreement is good for most systems studied.<sup>2</sup> We also notice that Persson and Baratoff predicted a decrease of 10% or more in the tunneling conductance for certain cases due to resonant processes,<sup>32</sup> and this is in accordance with our estimates of the inelastic effects.

So far, we have deliberately omitted the description of the Hamiltonian to be used in the present formalism since, in principle, any tight-binding-type Hamiltonian may be chosen. We would like to stress, however, that the entire STM is a rather complex system which involves both short-range interactions within each wire and long-range interactions ( $>5$  Å) between the sample surface and the tip apex. Therefore, it is not sufficient to achieve a good description of the isolated  $rs$  and  $at$  wires, but issues such as the surface wavefunction decay into the vacuum and the van der Waals attraction between the wires<sup>33–35</sup> play a crucial role and they must also be properly addressed if a quantitative comparison with the experiment is desired. The errors introduced by a particular Hamiltonian are difficult to estimate but, at least, it should always reproduce certain experimental facts (e.g., the exponential decay of the current with the tip-sample distance  $z$ <sup>2,36</sup> or the capability of the STM to resolve atoms in close-packed surfaces). In the forthcoming paper,<sup>23</sup> we will confirm that the simple extended Hückel theory<sup>37</sup> (EHT) already provides a fairly good qualitative description of the main processes that control the final contrast in the STM image. Furthermore, we find that the shape of the calculated images is hardly dependent on the exact electronic charge distribution at the surface blocks  $r$  and  $a$ ; i.e., images are not too sensitive to the precise electronic structure but, rather, they reflect its qualitative features.<sup>23</sup> Therefore, errors inherent to a particular Hamiltonian are less crucial when simulating STM images than when calculating, for instance, total energies or adsorption sites. This is in line with the fact that the STM has not yet been proved to be a powerful tool for determining electronic structures when compared to other spectroscopic techniques, despite some isolated applications such as the measurements of band gaps, metal work functions, or dispersion of surface bands.

In view of the above discussion, we cannot claim that the numerical values given above represent a realistic estimate of the overall accuracy of the method, but rather, they provide a lower limit to the error bars. In practice, once a particular Hamiltonian has been selected, the accuracy will be system dependent and, probably, a more reasonable way for its estimation is the direct comparison with experiment. It turns

out that for the systems studied, and employing the EHT, the calculated corrugations are at least within 50% of the experimental value, while we estimate a safe error bar in the absolute tip sample distance  $z$  to be  $1-2$  Å.<sup>23</sup>

These considerations imply that, even under the assumption that the structure of the system is well known, we cannot expect accurate quantitative results from our present formalism, and we consider it as a semiquantitative theory. Nevertheless, we do not feel it necessary at this point to introduce further refinements, since a crucial parameter in the images is the actual tip apex termination, and in the current STM experiments this cannot yet be determined easily. The associated uncertainty is probably overwhelming over the rest, emphasizing the need of fitting the apex geometry and chemical identity prior to extract any quantitative conclusions from the surface being probed. Many studies have provided evidence of this.<sup>9,16,38</sup> A related issue is the potential of STM to determine the surface crystallography (adsorption sites, bond lengths, buckling at the surface layer, etc.) via an experiment-theory fitting of the images and  $I(V)$  spectroscopic data. Previous ESQC applications have already obtained this kind of information in certain systems,<sup>14,18,16</sup> although a systematic way for evaluating the level of agreement between two images or  $I(V)$  curves has not yet been established.<sup>17</sup>

Having discussed above the shortcomings associated with the current theory, we conclude by highlighting its basic conceptual and practical aspects. In the first place, we have presented a semiempirical method capable of generating STM images in a fast and easy way; for a given set of tight-binding parameters, typical topographic images of entire unit cells take between 20 min and 2 h on a DEC Alpha Station. Most of the nonstructural parameters involved, such as the optical potential or the charge distribution, may be estimated prior to performing the calculation, so that, to a great extent, any agreement with the experiment cannot be considered as fortuitous or due to an excess in the number of parameters fitted. The use of the SGFM method allows one to take into account multiple-scattering effects at the interface in a quasixact way [the only related approximation is Eq. (65), which turns out to be very accurate]. If instead of the SGFM method, a first-order approximation in the number of tunneling events is used, then the resulting expressions for the total current can be decomposed into individual AO components or into contributions arising from a particular interaction at the interface and its interference with other tunneling paths. These type of decompositions permit a simple and comprehensive analysis of the origin of the contrast in the images. Furthermore, in employing the Büttiker-Landauer formula we fully couple the interface to the bulk materials; we should mention that this type of approach is becoming widely used in many studies of the conductance or  $I(V)$  characteristics of different nanodevices.<sup>6,12,22,24,39</sup> A very pleasant feature of the theory is the description of the whole system atom by atom, with relatively few geometrical restrictions, so that we are able to model the STM in a realistic way, inasmuch as the geometry of the constituent blocks is known *a priori*. On the other hand, the use of a tight-binding Hamiltonian makes feasible the study of large unit cells.

More importantly, the method can be applied to a wide variety of systems without the need for any modifications;

we may study different coadsorbed atoms or molecules, forming ordered or disordered structures, vacancies or impurities, steps, bias effects, etc. In particular, it represents a potential tool for identifying different chemical species at a surface during the STM experiments. The extension to semiconductor surfaces should not give any problems either as long as one includes band-bending effects, and these can readily be incorporated into the theory.

### ACKNOWLEDGMENTS

J. C. is delighted to acknowledge L. Chico for introducing him to the SGFM formalism, and for spending so many hours discussing its application to the conductance problem. We are also grateful to D. F. Ogletree and S. G. Louie for very useful discussions. J. C. acknowledges financial support from the Spanish Ministerio de Educación y Ciencia and from the Spanish CICYT under Contract No. PB94-1530. P. S. wishes to acknowledge CNRS International Collaboration Program PICS 240. This work was supported in part by the Director, Office of Energy Research, Office of Basic Energy Sciences, Materials Sciences Division of the U.S. Department of Energy under Contract No. DE-AC03-76SF00098.

### APPENDIX A: 1D SEMI-INFINITE CHAIN

In this appendix we derive explicit expressions for the transfer and Green function matrices of a semi-infinite 1D chain. Although most of the expressions to appear below can be found elsewhere (see, for example, Ref. 21), we prefer to include them here for the sake of completeness, and in order to provide a unified notation throughout the present work. We will only consider the  $rs$  chain of Fig. 1, while the equivalent relations for the  $at$  chain can be easily obtained by simply replacing  $r$  by  $a$  and  $s$  by  $t$  and also taking into account that propagation from surface to bulk within each chain has opposite signs (according to Fig. 1, positive for  $at$  and negative for  $rs$ ).

#### 1. Bulk Green function

We first consider the bulk chain  $s$  as infinite, so that the surface  $r$  is not present. In this case, and due to translation symmetry, the Green-function matrix blocks  $\mathcal{G}_{n'n}^0$  only depend on the difference  $n' - n$ . We may then substitute the subscript  $n$  by  $s$  and label these blocks as  $\mathcal{G}_{ss\pm n}^0$  or  $\mathcal{G}_{s\pm ns}^0$ . Projecting Eq. (18) at the diagonal block  $ss$ , we arrive at

$$I = F_{ss-1}\mathcal{G}_{s-1s}^0 + F_{ss}\mathcal{G}_{ss}^0 + F_{ss+1}\mathcal{G}_{s+1s}^0. \quad (\text{A1})$$

Making use of the  $T_{n'n}$  transfer matrices defined in Eq. (23) and again noting that they only depend on the difference  $n' - n$ , we may rewrite Eq. (A1) as

$$I = \{F_{ss-1}T_{s-1s} + F_{ss} + F_{ss+1}T_{s+1s}\}\mathcal{G}_{ss}^0, \quad (\text{A2})$$

which gives an expression for  $\mathcal{G}_{ss}^0$  as a function of  $T_{s\pm 1s}$ . To obtain these bulk transfer matrices we follow the iterative procedure developed in Ref. 40, which leads to the expressions

$$T_{s+1s} = t_0 + h_0t_1 + h_0h_1t_2 + \dots + h_0h_1 \dots h_{m-1}t_m, \quad (\text{A3})$$

$$T_{s-1s} = h_0 + t_0h_1 + t_0t_1h_2 + \dots + t_0t_1 \dots t_{m-1}h_m, \quad (\text{A4})$$

where  $m$  is the maximum iteration step used. The procedure is initialized through

$$t_0 = -(F_{ss})^{-1}F_{s+1s}, \quad (\text{A5})$$

$$h_0 = -(F_{ss})^{-1}F_{s-1s}, \quad (\text{A6})$$

while the rest of the  $h_i$  and  $t_i$  terms are obtained via

$$t_i = -(I - t_{i-1}h_{i-1} - h_{i-1}t_{i-1})^{-1}t_{i-1}^2, \quad (\text{A7})$$

$$h_i = -(I - t_{i-1}h_{i-1} - h_{i-1}t_{i-1})^{-1}h_{i-1}^2. \quad (\text{A8})$$

The algorithm is carried on until convergence in all matrix elements is achieved. Then, the diagonal bulk Green-function block  $\mathcal{G}_{ss}^0$  can be obtained by simply inverting the expression in brackets in Eq. (A2). The rest of the blocks  $\mathcal{G}_{s\pm ns}^0$  can be obtained by repeatedly multiplying  $\mathcal{G}_{ss}^0$  by the transfer matrices  $T_{s\pm 1s}$ ,

$$\mathcal{G}_{s\pm ns}^0 = (T_{s\pm 1s})^n \mathcal{G}_{ss}^0. \quad (\text{A9})$$

On the other hand, wave-function amplitudes at different PL's are simply related through

$$|a_{s\pm n}^0\rangle = (T_{s\pm 1s})^n |a_s^0\rangle. \quad (\text{A10})$$

If instead of projecting Eq. (18) we use Eq. (19), similar expressions may be obtained, but as a function of the  $S_{ss\pm 1}$  transfer matrices defined in Eq. (24) instead of the  $T_{s\pm 1s}$  matrices:

$$\mathcal{G}_{ss\pm n}^0 = \mathcal{G}_{ss}^0 (S_{ss\pm 1})^n. \quad (\text{A11})$$

Noting that in the bulk  $\mathcal{G}_{ss\mp n}^0 = \mathcal{G}_{s\pm ns}^0$ , we may combine Eqs. (A9) and (A11) to obtain a useful relation

$$(S_{ss\mp 1})^n (\mathcal{G}_{ss}^0)^{-1} = (\mathcal{G}_{ss}^0)^{-1} (T_{s\pm 1s})^n. \quad (\text{A12})$$

In fact, both transfer matrices are related through<sup>21</sup>

$$F_{ss\pm 1}T_{s\pm 1s} = S_{ss\pm 1}F_{s\pm 1s}. \quad (\text{A13})$$

#### 2. Surface Green function for a 1D chain

We now regard  $s$  as a semi-infinite chain, and allow for the existence of the surface  $r$ . Notice that in this case the translation symmetry is broken and the  $\mathcal{G}_{nn'}$  blocks depend on the actual value of  $n$  and  $n'$ . By projecting Eq. (18) at the diagonal block  $rr$ , we obtain

$$I = F_{rs}\mathcal{G}_{sr}^0 + F_{rr}\mathcal{G}_{rr}^0 = \{F_{rs}T_{sr} + F_{rr}\}\mathcal{G}_{rr}^0, \quad (\text{A14})$$

where we have introduced the transfer matrix  $T_{sr}$  defined as

$$T_{sr} = \mathcal{G}_{sr}^0 (\mathcal{G}_{rr}^0)^{-1}. \quad (\text{A15})$$

In order to evaluate the surface Green function  $\mathcal{G}_{rr}^0$  we then need to find  $T_{sr}$  first. To this end, we project Eq. (18) on the matrix block  $sr$  to obtain

$$\begin{aligned}
0 &= F_{sr} \mathcal{G}_{rr}^0 + F_{ss} \mathcal{G}_{sr}^0 + F_{ss-1} \mathcal{G}_{s-1s}^0 \\
&= F_{sr} \mathcal{G}_{rr}^0 + \{F_{ss} + F_{ss-1} T_{s-1s}\} \mathcal{G}_{sr}^0. \quad (\text{A16})
\end{aligned}$$

Notice that we can still use in this expression the bulk transfer matrix  $T_{s-1s}$  deduced above, since the coupling of PL  $n = -2$  with the rest of the bulk  $s$  chain ( $n < -2$ ) is not affected by the presence of the surface  $r$ , which is located at the other side ( $n = -1$ ).

Combining Eqs. (A15) and (A16), we can now find an explicit expression for  $T_{sr}$ :

$$T_{sr} = -\{F_{ss} + F_{ss-1} T_{s-1s}\}^{-1} F_{sr}. \quad (\text{A17})$$

We may arrive at a similar relation for  $\mathcal{G}_{rr}^0$  by using Eq. (19) to perform the projections:

$$I = \mathcal{G}_{rr}^0 \{F_{rr} + S_{rs} F_{sr}\}, \quad (\text{A18})$$

where the  $S_{rs}$  transfer matrix is defined as

$$S_{rs} = (\mathcal{G}_{rr}^0)^{-1} \mathcal{G}_{rs}^0, \quad (\text{A19})$$

and may be obtained by projecting Eq. (19) at  $rs$ :

$$\begin{aligned}
0 &= \mathcal{G}_{rr}^0 F_{rs} + \mathcal{G}_{rs}^0 F_{ss} + \mathcal{G}_{rs-1}^0 F_{s-1s} \\
&= \mathcal{G}_{rr}^0 F_{rs} + \mathcal{G}_{rs}^0 \{F_{ss} + S_{ss-1} F_{s-1s}\}. \quad (\text{A20})
\end{aligned}$$

With the aid of Eq. (A13) the calculation of the bulk transfer matrices  $S_{ss\pm 1}$  can be avoided, and, from Eqs. (A19) and (A20)  $S_{rs}$  can be expressed as

$$S_{rs} = -F_{rs} \{F_{ss} + F_{ss-1} T_{s-1s}\}^{-1}. \quad (\text{A21})$$

Finally, the local density of states projected on an orbital  $\alpha_i$  at layer  $n$ ,  $\rho_n^0(\alpha_i)$ , may be obtained directly from the Green function through<sup>41</sup>

$$\rho_n^0(\alpha_i) = -\frac{1}{\pi} \text{Im}\{(\mathcal{G}O)_{n,n}(\alpha_i, \alpha_i)\}, \quad (\text{A22})$$

where  $\text{Im}$  stands for the imaginary part and  $O$  is the overlap matrix. Notice that Eq. (A22) involves the products  $\mathcal{G}_{nn\pm 1} O_{n\pm 1n}$  besides the diagonal term  $\mathcal{G}_{nn} O_{nn}$ . The total LDOS projected on a PL  $n$ ,  $\rho_n^0$ , is then simply given by

$$\rho_n^0 = \sum_i^{N_\alpha} \rho_n^0(\alpha_i) = -\frac{1}{\pi} \text{Tr}\{\text{Im}(\mathcal{G}O)_{nn}\}, \quad (\text{A23})$$

where  $\text{Tr}$  is the trace of the matrix.

## APPENDIX B: ANALYTICAL DERIVATION OF $\mathcal{T}(E)$

In this appendix we wish to find an analytical expression for the transmission coefficient  $\mathcal{T}(E)$  for the simple 1D system depicted in Fig. 3. Let us first find  $\mathcal{G}_{ra}$ . Inserting Eqs. (41)–(45) into Eq. (20) and using definitions  $q = (E - e)/h$ ,  $X = (\omega - e)/h$ ,  $Y = \alpha/h$ , and  $Z = \beta/\alpha$ , we have

$$\mathcal{G}_{ra} = \frac{-\beta}{|(\mathcal{G}_{rr}^0)^{-1}|} = \frac{-\beta}{h^2[(q+t)(q-X+Y^2t) - Y^2Z^2]}. \quad (\text{B1})$$

Now we may calculate explicitly the scattering coefficient  $S^+(E)$  in Eq. (40). Taking into account that  $(U_t^+)^{-1} U_s^+ = 1$  and dropping the  $T_{ta} = t$  term since it only provides a phase factor, we obtain

$$S^+(E) = \frac{-Y^2 Z t (q + 2t)}{(q+t)(q-X+Y^2t) - Y^2 Z^2}. \quad (\text{B2})$$

In order to find the squared modulus of this expression, it is convenient to distinguish real and imaginary parts. Since all quantities in Eq. (B2) are real except  $t$ , we write  $t = -q/2 \pm \Delta$ , where  $\Delta = \sqrt{q^2 - 4}$  is a purely imaginary quantity. Dropping again the  $t$  in the numerator of Eq. (B2) and using the definition of  $\Delta$ , we obtain

$$S^+(E) = \frac{-Y^2 Z (\pm \Delta)}{(q/2 \pm \Delta/2)[q - X + Y^2(-q/2 \pm \Delta/2)] - Y^2 Z^2}, \quad (\text{B3})$$

and after some algebra we may separate those terms multiplying  $\Delta$  from the rest through

$$(S^+(E))^{-1} = -\frac{(1/Z + Z)}{4W^2} \left\{ (q - X) + \frac{q^2 - qX - 4W^2}{\pm \Delta} \right\}, \quad (\text{B4})$$

where we have defined  $W = Y\sqrt{(1+Z^2)/2}$ . The  $(q - X)$  term inside the braces is real, and the second purely imaginary, so that we can now easily evaluate the transmission coefficient according to

$$\mathcal{T}(E) = \{[\text{Re}(1/S)]^2 + [\text{Im}(1/S)]^2\}^{-1}. \quad (\text{B5})$$

By substituting Eq. (B4) into Eq. (B5), we obtain

$$\mathcal{T}(E) = \mathcal{T}_1 \mathcal{T}_2(E), \quad (\text{B6})$$

where

$$\mathcal{T}_1 = \frac{4}{(1/Z + Z)^2}, \quad (\text{B7})$$

while the second factor  $\mathcal{T}_2(E)$  is given by

$$\mathcal{T}_2(E) = (4W^4) \left( (q - X)^2 + \frac{(q^2 - qX - 4W^2)^2}{4 - q^2} \right)^{-1}, \quad (\text{B8})$$

and after some rearrangement one finally finds

$$\mathcal{T}_2(E) = \left( 1 + \frac{[X + q(W^2 - 1)]^2}{W^4(4 - q^2)} \right)^{-1}. \quad (\text{B9})$$

\*Permanent address: Instituto de Ciencia de Materiales de Madrid, CSIC, Cantoblanco, 28049 Madrid, Spain.

†Author to whom correspondence should be addressed. Electronic address: vanhove@Csa2.LBL.Gov

<sup>1</sup>J. Tersoff and D.R. Hamann, Phys. Rev. B **31**, 805 (1985).

<sup>2</sup>R. Wiesendanger and H.-J. Güntherodt, *Scanning Tunneling Microscopy III* (Springer-Verlag, Berlin, 1993).

<sup>3</sup>P. Sautet and C. Joachim, Phys. Rev. B **38**, 12 238 (1988).

- <sup>4</sup>P. Sautet and C. Joachim, *Chem. Phys. Lett.* **185**, 23 (1991).
- <sup>5</sup>N. Mingo *et al.*, *Phys. Rev. B* **54**, 2225 (1996).
- <sup>6</sup>V. Mujica, M. Kemp, and M.A. Ratner, *J. Chem. Phys.* **101**, 6849 (1994); **101**, 6856 (1994); M. Kemp, A. Roitberg, V. Mujica, T. Wanta, and M.A. Ratner, *ibid.* **100**, 8350 (1996).
- <sup>7</sup>J.A. Stroschio, R.M. Feenstra, and A.P. Fein, *Phys. Rev. Lett.* **58**, 1668 (1987).
- <sup>8</sup>I.-W. Lyo and Ph. Avouris, *Science* **245**, 1369 (1989).
- <sup>9</sup>M. Tsukada, K. Kobayashi, and N. Isshiki, *Surf. Sci. Rep.* **13**, 265 (1991).
- <sup>10</sup>M.F. Crommie, C.P. Lutz, and D.M. Eigler, *Nature (London)* **363**, 524 (1993); L.C. Davies, M.P. Everson, and R.C. Jaklevic, *Phys. Rev. B* **43**, 3821 (1991).
- <sup>11</sup>D.M. Eigler and E.K. Schweizer, *Nature (London)* **344**, 524 (1990); J. Cerdá, P.L. de Andres, F. Flores, and R. Perez, *Phys. Rev. B* **45**, 8721 (1992); X. Bouju, C. Joachim, C. Girard, and P. Sautet, *ibid.* **47**, 7454 (1993).
- <sup>12</sup>M. Brandbyge *et al.*, *Phys. Rev. B* **52**, 8499 (1995).
- <sup>13</sup>C.C. Williams and H.K. Wickramasinghe, *Nature (London)* **344**, 317 (1990); J.A. Stóvneng and P. Lipavský, *Phys. Rev. B* **42**, 9214 (1990).
- <sup>14</sup>M.L. Bocquet and P. Sautet, *Surf. Sci.* **360**, 28 (1996).
- <sup>15</sup>P. Sautet, *Surf. Sci.* **374**, 406 (1997).
- <sup>16</sup>P. Sautet, J.C. Dunphy, D.F. Ogletree, and M. Salmeron, *Surf. Sci.* **295**, 347 (1993); P. Sautet *et al.*, *Surf. Sci.* **315**, 127 (1994).
- <sup>17</sup>J.C. Dunphy, P. Sautet, D.F. Ogletree, and M. Salmeron, *Phys. Rev. B* **52**, 11 446 (1995); P. Sautet, J.C. Dunphy, and M. Salmeron, *Surf. Sci.* **364**, 335 (1996).
- <sup>18</sup>P. Sautet and M.L. Bocquet, *Surf. Sci.* **304**, L445 (1994); *Phys. Rev. B* **53**, 4910 (1996).
- <sup>19</sup>M. Büttiker, Y. Imry, R. Landauer, and S. Pinhas, *Phys. Rev. B* **31**, 6207 (1985).
- <sup>20</sup>D.H. Lee and J.D. Joannopoulos, *Phys. Rev. B* **23**, 4988 (1981).
- <sup>21</sup>F. García-Moliner and V.R. Velasco, *Theory of Single and Multiple Interfaces* (World Scientific, Singapore, 1992); M.C. Muñoz, V.R. Velasco, and F. García-Moliner, *Prog. Surf. Sci.* **26**, 117 (1987).
- <sup>22</sup>L. Chico, L.X. Benedict, S.G. Louie, and M.L. Cohen, *Phys. Rev. B* **54**, 2600 (1996).
- <sup>23</sup>J. Cerdá, A. Yoon, M.A. Van Hove, P. Sautet, M. Salmeron, and G.A. Somorjai, following paper, *Phys. Rev. B* **56**, 15 900 (1997).
- <sup>24</sup>T.N. Todorov, G.A.D. Briggs, and A.P. Sutton, *J. Phys.: Condens. Matter* **5**, 2389 (1993).
- <sup>25</sup>A.D. Stone and A. Szafer, *IBM J. Res. Dev.* **32**, 384 (1988).
- <sup>26</sup>D.S. Fisher and P.A. Lee, *Phys. Rev. B* **23**, 6851 (1981).
- <sup>27</sup>R. Ramirez and M.C. Böhm, *Int. J. Quantum Chem.* **30**, 391 (1986).
- <sup>28</sup>M.A. Van Hove, W.H. Weinberg, and C.M. Chan, *Low Energy Electron Diffraction* (Springer-Verlag, Berlin, 1986).
- <sup>29</sup>R. García, J.J. Sáenz, J.M. Soler, and N. García, *Surf. Sci.* **181**, 69 (1987); A.D. Stone and P.A. Lee, *Phys. Rev. Lett.* **54**, 1196 (1985).
- <sup>30</sup>R.E. Walkup, D.M. Newns, and Ph. Avouris, *Phys. Rev. B* **48**, 1858 (1993); T. Shimizu, K. Kobayashi, and M. Tsukada, *Appl. Surf. Sci.* **60-61**, 454 (1992); J.A. Stóvneng, E.H. Hauge, P. Lipavský, and V. Spicka, *Phys. Rev. B* **44**, 13 595 (1991).
- <sup>31</sup>V. Mujica, M. Kemp, A. Roitberg, and M.A. Ratner, *J. Chem. Phys.* **104**, 7296 (1996).
- <sup>32</sup>B.N.J. Persson and A. Baratoff, *Phys. Rev. Lett.* **59**, 339 (1987).
- <sup>33</sup>Y. Andersson, D.C. Langreth, and B.I. Lundqvist, *Phys. Rev. Lett.* **76**, 102 (1996).
- <sup>34</sup>H. Kageshima and M. Tsukada, *Phys. Rev. B* **46**, 6928 (1992).
- <sup>35</sup>J. Tersoff, *Phys. Rev. B* **40**, 11 990 (1989).
- <sup>36</sup>L. Olesen *et al.*, *Phys. Rev. Lett.* **76**, 1485 (1996).
- <sup>37</sup>J.H. Ammeter, H.-B. Bürgi, J.C. Thibeault, and R. Hoffmann, *J. Am. Chem. Soc.* **100**, 3686 (1978).
- <sup>38</sup>C.J. Chen, *Phys. Rev. Lett.* **69**, 1656 (1992).
- <sup>39</sup>See, for example, M. Morifuji and C. Hamaguchi, *Phys. Rev. B* **52**, 14 131 (1995); C. Bruder, R. Fazio, and H. Schoeller, *Phys. Rev. Lett.* **76**, 114 (1996); M.P. Samanta *et al.*, *Phys. Rev. B* **53**, R7626 (1996).
- <sup>40</sup>M.P. López Sancho, J.M. López Sancho, and J. Rubio, *J. Phys. F* **14**, 1205 (1984); **15**, 851 (1985).
- <sup>41</sup>M.P. López Sancho, J.M. López Sancho, and J. Rubio, *J. Phys. C* **18**, 1803 (1985).